Sustainable Energy, Grids and Networks 43 (2025) 101899

Contents lists available at ScienceDirect

Sustainable Energy, Grids and Networks

journal homepage: www.elsevier.com/locate/segan

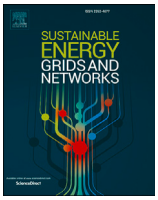

Optimal charging strategy for electric trucks with vehicle-to-grid at a wind-powered electric vehicle charging hub

Alphonse Francis[a], Matteo Fresia[a], Edoardo Barabino[b], Stefano Bracco[a,*]

[a] Department of Electrical, Electronic, Telecommunications Engineering and Naval Architecture, University of Genova, Via Opera Pia 11a, Genova, 16145, Italy
[b] FERA(Fabbrica Energie Rinnovabili Alternative) Srl, Piazza Cavour 7, Milan, 20121, Italy

HIGHLIGHTS

- Energy management system for an electric vehicle charging hub fed by a large-scale wind farm.
- Assessment of the role of BESS in minimizing operating cost and CO_2 emissions.
- Assessment of the impact of smart charging and Vehicle-to-Grid (V2G) on the operation of the hub under different operating conditions, especially during BESS faults.
- Accurate implementation of inverter capability curves to model reactive power sharing.
- Application to a real electric vehicle charging hub located in Vado Ligure, Italy.

ARTICLE INFO

Keywords:
Electric trucks
Electric vehicle charging hub
Vehicle-to-grid
Capability curves
Energy management system
Wind farm

ABSTRACT

The transportation sector is a major contributor to greenhouse gas emissions. To address this, the European Union is promoting the integration of Electric Vehicle (EV) charging infrastructures with Renewable Energy Sources (RESs). The intermittency of RESs can be mitigated through the use of Battery Energy Storage Systems (BESSs) and advanced EV charging strategies such as Vehicle-to-Grid (V2G), which require effective energy management. Accurate implementation of RES inverter capability curves is essential to minimize discrepancies between theoretical models and real-world performance. This study presents an Energy Management System (EMS) based on a Mixed Integer Linear Programming (MILP) model to optimize overnight charging of electric trucks at an Electric Vehicle Charging Hub (EVCH) powered by RESs. The EMS is developed in Matlab/Yalmip and solved using Gurobi. The model is applied to a real EVCH connected to a large-scale wind farm in Liguria, Italy, with integration of Photovoltaic (PV) and BESS units. Validation is performed through comparison with HOMER Grid simulations. Several sensitivity analyses are conducted, varying RES availability, truck presence, and electricity prices, to assess EVCH performance. Results show that V2G enables a 13.3 % cost reduction compared to constant-power charging. If the BESS is out of service, the increase in facility net costs is limited to 3.6 %. However, if trucks are available during the day, the V2G benefit is nullified due to overlap with RES production peaks. Conversely, higher electricity prices lead to a 6.7 % increase in the V2G contribution.

1. Introduction

1.1. Motivation and background

The reduction of CO_2 and other Greenhouse Gas (GHG) emissions from the transportation sector, which accounts for almost 26 % of the GHG emissions at European level, has been one of the major goals of the “Fit for 55” package, announced by the European Union (EU) [1,2]. The outcomes are the promotion of the use of Zero Emission Vehicles (ZEVs), especially Electric Vehicles (EVs), and significant increase in the use of Renewable Energy Sources (RESs) in the transportation sector. Heavy duty vehicles contribute to a quarter of the emissions from the road transportation sector [3], with trucks representing 85 % of the total emissions followed by passenger transport vehicles [2]. Goals have been defined for the complete reduction of GHG emissions from new

* Corresponding author.
Email address: stefano.bracco@unige.it (S. Bracco).

https://doi.org/10.1016/j.segan.2025.101899
Received 23 December 2024; Received in revised form 5 May 2025; Accepted 1 August 2025
Available online 5 August 2025

cars, buses, vans and trucks [4]. Policy proposals are being developed by the member states of the EU to encourage the use of Heavy Electric Vehicles (HEVs) for goods transport [5]. Studies reveal that the use of electric trucks in the reduction of GHG emissions is effective in the long run when coupled with long term electrification of road transport scenarios [6]. Although the growth of electric truck and bus sales in the EU has seen a surge, they account for only less than 1 % of the total sales of the EVs [7] as the evolving technology, the limited charging infrastructure and the high battery costs can be held responsible for the hesitation in the use of electric trucks for freight movement [8]. Consequently, an increase in the development of EV fast-charging infrastructure represents a crucial challenge to sustain the energy transition.

The use of RESs to power HEVs is crucial in preventing the shift of the emissions from the transportation sector towards the power generation sector. Inclusion of RESs for power generation falls in line with the sustainable development and climate goals of the EU. Photovoltaic (PV) and Wind Turbines (WTs) power plants represent the most common solutions exploited both at small and utility scales [9]. These plants are connected to local facilities through inverters, to maximize primary self consumption: nevertheless, inverters are unable to ensure the same performance in frequency and voltage regulation as static generators on their own, due to their inherent characteristics (being static generators, overloading capability, etc.), therefore, the use of smart inverters with dedicated controllers enables RES power plants to exchange reactive energy with loads in microgrids [10] as well as with the public network, which is crucial in maintaining control over voltage [11,12]. In fact, during peak production periods, RESs could induce overvoltage transients that may result in issues for the stable operation of the local distribution network [13].

Within this framework, Energy Storage Systems (ESSs), particularly Battery Energy Storage Systems (BESSs) provide crucial system flexibility for RES integration [14]. Besides enhancing energy security [15], BESSs can participate in peak shaving [16] and offer the advantage of providing ancillary services [17,18]. Moreover, BESSs are useful to ensure safe operations of microgrids, as reported in [19]. Calendar and cycling aging processes are detrimental to the operating life of BESSs with the latter related to the number of charging and discharging cycles, contributing the most towards reducing the operational life of storage systems as reported in the studies [20], and [21], which developed aging models for BESSs. The impact of Vehicle-to-Grid (V2G) technique on battery degradation is also explored in [22] and [23].

The complete transition to ZEVs is imminent in the urban freight and passenger transport sector, as the emission standards are tightened by the EU [24]. EVs can be considered as mobile BESSs, therefore providing further flexibility services [25]. Nevertheless, similar to RES generators, massive penetration of EV fleets could induce problems in terms of voltage stability, in case of large peaks of charging demand [26]. In addition, HEV battery capacities typically range between 350 kWh and 550 kWh and require higher charging powers when compared to light EVs, further worsening possible voltage issues: in fact, fast charging of these EVs is expected to add additional peaks in the load demand profile while creating congestion problems for the distribution system operators. Exploiting V2G and Vehicle-to-Building (V2B) functionalities, using the battery capacities of HEV fleets, can help mitigate demand peaks in the utility grid and can provide economic and environmental benefits. While [27] discusses smart charging strategies for HEVs, [28] and [29] explore the profitability of the V2G charging strategies of heavy electric vehicles and [30] optimizes the production process in a facility by integrating electric trucks, exploiting their V2G functionality. Moreover, EVs can be integrated into energy communities [31], providing further flexibility to the system in terms of avoided transmission losses.

1.2. Literature review

Effective energy management is significant when RESs are integrated with electric mobility systems. Examples of Energy Management Systems (EMSs) based on the Mixed Integer Linear Programming (MILP) approach for the optimal operation of electric mobility facilities are available in the literature. Reference [32] provides an optimal scheduling approach for a charging station of both electric and hydrogen-fed vehicles, with local hydrogen production through the use of electrolyzers: nevertheless, electricity comes from the distribution network and RESs are not considered to be installed at the facility, therefore not assessing their impact in an electric vehicle charging station. In [33] the impact of PV installation in an EV charging station close to a retail store is discussed, showing great potential in terms of satisfaction of EV charging demand: however, the possibility of applying V2G technology is not assessed. V2G functionality is instead explored in [34], where a parking lot equipped with a PV system along with a BESS aims to minimize the operating costs by reducing the dependence on the utility grid. The household EMS presented in [35] exploits the V2B functionalities of EVs to minimize the net costs related to the purchase and sale of energy from/to the public network by scheduling the charging and discharging operations of EVs and the operations of shiftable electrical loads connected to the grid. In [36], the scheduling of electricity-intensive household appliances is optimized to align with the power generation from distributed energy sources during periods of higher electricity tariffs, effectively minimizing the CO_2 emissions associated with power absorbed from the public grid. The MILP model in [37] provides a structured framework to integrate renewable energy into the public network and optimize the BESS operations and the scheduling of diesel generators in a microgrid, targeting cost minimization in both grid-connected and islanded modes. The MILP model in [38] proposes optimal dispatch solution for the operation of BESS in a nanogrid while simultaneously optimizing the size of the BESS. In [39], the MILP-based EMS effectively manages the operations in a hydrogen-based renewable energy community and performs effective scheduling of electrolyzers, hydrogen tanks, and fuel cells with the aim of minimizing the total operating costs.

A comparison of the impact of MILP and Markov's decision process approaches on the effectiveness of EMS in maximizing the profits in an EV charging station is presented in [40], with the MILP approach providing better results. A battery usage cost is added to the objective function of the EMS in [41] to optimize the operations of BESS for a longer operating life while maximizing the profits in an EV charging station coupled with a PV system. In [42] and [43], linearized constraints for RES inverters that allow the exchange of both active and reactive power are presented so that the EMS reduces the dependence on the grid for the optimal operation of a prosumer building integrated with RES and charging points for an EV fleet. A cost-effective management strategy is presented in [44] where a MILP model optimizes the operations of a combined cooling, heat, and power system supplying the power and cooling demand of data centers. In [45], the EMS optimizes the interaction of the utility grid, PV system, electrolyser and BESS to schedule the charging of ZEVs within an all-in-one EV charging station with hydrogen filling and battery swapping. An EMS designed to optimize the operations of a community-based prosumer microgrid is described in [46] where the EV availability is modeled using the Markov chain model. An approach for the optimal operation of an industrial microgrid with a centralized BESS, PV plants and EV charging points is discussed in [47], considering two EV cars and two EV trucks for freight delivery. The considered industrial user is supposed to be a member of a renewable energy community located in Italy: therefore, the member has to modulate the exchange of active power with the network in accordance with a reference profile provided by the community aggregator to maximize the shared energy within the community and the relevant incentive. In [48], a multi-objective optimization model is presented where the V2G capability of EVs is utilized in reducing the CO_2 emissions from the utility grid related to the production of electricity from fossil fuels. A taxonomy table highlighting the research gaps in the relevant literature is presented in Table 1. The table categorizes the aforementioned sources according to the considered generation resources (PV, WT, BESS), types of EVs (EV cars, EV trucks), possible penalties regarding the unsatisfied charging

Table 1
Summary of the literature review.

Ref.	PV	WT	BESS	EV Cars	EV Trucks	Penalty on departure SOC unsatisfaction	V2G	Reactive power	Application scale
[32]	–	–	✓	✓	–	–	–	–	Charging hub – Few MW
[33]	✓	–	–	✓	–	–	–	–	Supermarket – <1 MW
[34]	✓	–	✓	✓	–	✓	✓	–	Parking station – <1 MW
[35]	✓	–	✓	✓	–	✓	✓	–	House – some kW
[40]	✓	✓	✓	✓	–	–	✓	–	Parking station – <1 MW
[41]	✓	–	✓	✓	–	–	–	–	Charging station – <1 MW
[42,43]	✓	✓	–	✓	–	–	✓	✓	Charging station for postal building – <1 MW
[45]	✓	–	–	✓	–	–	✓*	–	Charging station – <1 MW
[46]	✓	–	✓	✓	–	–	✓	–	Microgrid - Few kW
[47]	✓	–	✓	✓	✓	–	✓	–	Industrial Microgrid – <1 MW
This study	✓	✓	✓	✓	✓	✓	✓	✓	Charging station – ≈ 10 MW

*Battery swapping technique used

demand (i.e., the EV leaves the EVCH with a SOC lower than the desired one), application of V2G, modeling of reactive power exchanges and application scale.

1.3. Problem overview and contributions

While existing studies primarily focus on small-scale charging stations with no local RES generation or powered by small RES power plants, they often fail to provide substantial environmental benefits or scalable solutions for heavy-duty EVs. Moreover, few studies explore the integration of fast-charging infrastructure for electric trucks with V2G capabilities, assessing the impact of this service on economic and energy performance of charging stations. In addition, reactive power management is usually neglected in literature. Finally, to the best of the authors' knowledge, very few studies rely on real-world data derived from an existing charging hub. Within this state of the art, the present study aims to develop a MILP-based EMS to be applied to optimize the operation of an Electric Vehicle Charging Hub (EVCH) located in Vado Ligure, a city in the Northern Italian region of Liguria. The hub, capable of hosting both private electric cars and electric trucks, is owned by Ricarica s.r.l. (from now on, "*Ricarica*"), a subsidiary of Fera s.r.l. (from now on, "*Fera*"). The EVCH is equipped with three charging stations (2×350 kW $+ 1 \times 75$ kW), able to provide fast charging, directly under the ownership of *Ricarica*, being able to satisfy the charging demand of both cars and trucks, while another twelve charging stations (12×250 kW) are installed at the facility under the ownership of another operator. The EVCH is directly connected, through a dedicated connection, to a WT farm, composed of 4 large-scale WTs, under the ownership of *Fera*, installed in the nearby hills with a total rated power of 9.4 MW. This direct connection between the wind farm and the EVCH makes the facility a unique case study at the European level. The EVCH is also connected to the utility grid through a Medium Voltage (MV) connection. The hub is being upgraded to host a commercial building along with a PV power plant and a BESS.

The proposed EMS model is validated by comparing its results with those of an optimization model developed in HOMER Grid. Moreover, a comparison of cost performances in case of application of traditional constant-power charging, smart charging and V2G is performed. Two base scenarios are considered, assuming that an EV truck is parked at the facility for overnight charging: in the first scenario, V2G is considered (although not currently implemented at the EVCH), in order to assess the impact of advanced charging techniques on the operations of the facility, while a second scenario considers the BESS to be out of service, in order to assess how the operation of the EVCH changes without the flexibility provided by the storage system. The second scenario is further analysed through several sensitivity analyses that assess the impact that high/low wind and solar energy availability, daytime/nighttime electric truck availability and high/low electricity prices have on the operation of the facility.

The objective of the EMS is to effectively manage the RES power plants to minimize the net operating costs of the hub, which include the costs related to the exchange of active and reactive energy with the utility grid, the costs related to peak power absorption from the grid, the possible penalty due to unsatisfaction of the charging demand of the electric truck and the costs related to BESS operation.

This study extends the results of the previous research [49] and its contributions are:

- Definition of a day-ahead EMS for the optimal operation of an EVCH directly connected to a large scale wind farm, participating to day-ahead market.
- Application of the EMS to a real-world case, exploiting actual data from the EVCH in Vado Ligure. In fact, data about EV presence and EV charging demand at the EVCH for each time interval of the time horizon have been derived by the data provided to the authors by *Fera* and *Ricarica*, along with the production of the 4 WTs.
- Analysis of the impact of V2G applied to electric trucks. To this purpose, two scenarios are considered, one with the BESS in operation and one with the BESS out of service, to identify potential advantages of exploiting V2G in different operating conditions.
- Comparison of economic performance of the EVCH considering the application of different charging techniques (traditional constant-power charging, smart charging and V2G) and charging power levels (quick charging vs. fast charging) for the electric truck.
- Set up of sensitivity analyses performed considering high/low RES production, daytime/nighttime electric truck presence at the EVCH and high/low electricity prices, to further assess the impact of V2G under different operating conditions.
- Evaluation of the impact of the EVCH on the economic performance of the wind farm, given the presence of multiple EV operators.
- A comprehensive approach accounting for both active and reactive power, presenting an innovative and accurate approach to linearize the capability curves of BESS and inverters, to ensure the global optimality of the solution.

Indeed, to the best of the author's knowledge, the present study is one of the first regarding EVCHs allowing the fast charging of electric trucks, with the possibility of applying V2G technique. In fact, other studies in literature either consider small-scale EV charging stations fed by the local distribution grid, therefore not providing environmental benefits, or by small-scale local RES generators with limited potential: instead, the present paper provides a case study of an EVCH directly connected to a large-scale WT power plant, through a dedicated connection.

The remainder of the paper is organized as follows: Section 2 describes the charging hub; Section 3 presents the mathematical model of the EMS; the results are discussed in Section 4, while Section 5 draws the main conclusions of the study.

Fig. 1. The *Fera* Windfarm and the *Ricarica* EV chargers.

2. Facility description

A brief description of the EVCH under study along with the proposed technological upgrades is presented in the following sections.

2.1. Vado ligure EVCH

The EVCH under study is located in the town of *Vado Ligure*, which falls under the province of *Savona* of the Ligurian region of Italy. The "*Rocche Bianche*" hills in Vado Ligure host a 9.4 MW wind farm, commissioned by *Fera* in April 2020. The EVCH launched in June 2023 by *Ricarica*, a division of *Fera*, is directly connected to the wind farm: the facility represents the first example in Italy of an EVCH directly connected to a large-size RES power plant. The hub is located in an industrial area, close to a highway exit and is connected to the public distribution network through a MV/LV substation. It currently hosts EV charging stations managed by two operators – *Ricarica* and another EV charging service provider (hereinafter referred to as "*Operator* 2"). EV charging stations of both operators support fast charging of vehicles. *Ricarica* hosts chargers of two types, "type *a*" and "type *b*". The "type *a*" Direct Current (DC) ultra-fast chargers have a rated capacity of 350 kW and support Combined Charging System (CCS) with Combo2 (CCS2) connectors. The "type *b*" DC fast chargers have a rated capacity of 75 kW and support a CHAdeMo connector along with the CCS2 plug. Two "type *a*" and one "type *b*" chargers are present at the facility. Both types of chargers can be used for the fast charging of electric trucks, vans as well as light EVs. A visitors' lounge for the users of the facility is located in the old office building present at the hub. The EV chargers of *Ricarica* and the WTs owned by *Fera* are shown in Fig. 1.

2.2. Planned upgrades of the facility

The facility is to be renovated in the near future and the improved hub would host a multi-storeyed energy efficient building with offices of *Fera* and *Ricarica* along with commercial outlets, a restaurant and a modern museum of EVs. Heat pumps will be designed to satisfy the hot water, heating and cooling demands of the building. A PV power plant will be installed on the rooftop; a BESS will be installed too, in order to increase the self-consumption of RESs, as well as to provide flexibility of supply. The electrical loads of the building are assumed to be inductive while the EVs are supposed not to exchange reactive power with the facility. Additionally, given its specific location in an industrial area, the hub provides overnight charging for electric trucks parked at the facility, with the willingness to increase the number of chargers for trucks. These additions to the existing hub infrastructure call for effective management of the technologies to minimize the daily operating costs of the hub. A simplified layout of the EVCH is presented in Fig. 2.

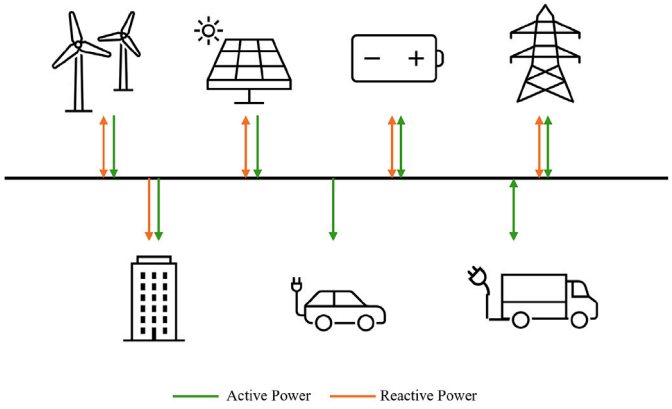

Fig. 2. Simplified layout of the proposed hub.

3. Mathematical model

The present section fully details and discusses the mathematical model of the optimization problem. The objective of the EMS is to manage the RES power plants to minimize the daily operating costs of the EVCH, while ensuring that the energy demand of the building and of the EVs is satisfied and guaranteeing that the electric trucks present overnight at the facility are smartly charged and reach the desired State of Charge (SoC) at the time of departure. The optimization horizon is divided into T intervals of duration Δ and t indicates the generic time interval of the optimization problem. The constraints describing the behaviour of the technologies present at the EVCH and the objective function are discussed in the sections below.

3.1. BESS and Grid model

3.1.1. BESS

The active power charged to the BESS, $P_t^{B,ch}$ and the active power discharged by the BESS, $P_t^{B,dch}$, are continuous decision variables and are limited by the size of the BESS inverter, $A^{in,B}$, which is an input data, as described in the constraints below.

$$0 \leq P_t^{B,ch} \leq A^{in,B} \cdot x_t^{B,ch} \quad \forall t = 1, \dots, T \tag{1}$$

$$0 \leq P_t^{B,dch} \leq A^{in,B} \cdot x_t^{B,dch} \quad \forall t = 1, \dots, T \tag{2}$$

$$x_t^{B,ch} + x_t^{B,dch} \leq 1 \quad \forall t = 1, \dots, T \tag{3}$$

In (1) and (2), $x_t^{B,ch}$ and $x_t^{B,dch}$ are binary decision variables that are equal to 1 when the BESS is charging or discharging respectively and set to 0 otherwise. Thus, the occurrence of simultaneous charge and discharge cycles is forbidden, as in constraints (3).

The continuous decision variables E_t^B, which represent the energy content of BESS, are governed by a discrete time-dependent energy balance, which takes into account the self-discharge rate, λ, along with the charging and discharging efficiencies, η_{ch}^B and η_{dch}^B respectively, which are inputs to the model. The constraints related to the energy content of the BESS are reported below.

$$E_{t+1}^B = (1-\lambda) \cdot E_t^B + \Delta \cdot \left(\eta^{B,ch} \cdot P_t^{B,ch} - \frac{P_t^{B,dch}}{\eta^{B,dch}} \right) \quad \forall t = 1, \dots, T-1 \tag{4}$$

$$SoC^{min} \cdot C^B \leq E_t^B \leq SoC^{max} \cdot C^B \quad \forall t = 1, \ldots, T \tag{5}$$

$$E_1^B = SoC^{ini} \cdot C^B \tag{6}$$

To prolong the operational life of the BESS, the energy content must be maintained between a specified minimum and maximum SoC, SoC^{min} and SoC^{max}, as outlined in constraints (5), where C^B represents the rated capacity of the BESS. The EMS assigns an initial SoC, SoC^{ini}, at the start of the optimization horizon as specified in constraint (6). Cycling aging is limited by minimizing the number of cycles, as reported in the constraints below.

$$x_{t+1}^{B,ch} - x_t^{B,ch} \leq x_t^{B,ch,str} - x_t^{B,ch,end} \quad \forall t = 1, \ldots, T-1 \tag{7}$$

$$x_{t+1}^{B,dch} - x_t^{B,dch} \leq x_t^{B,dch,str} - x_t^{B,dch,end} \quad \forall t = 1, \ldots, T-1 \tag{8}$$

$$x_t^{B,ch,str} + x_t^{B,ch,end} \leq 1 \quad \forall t = 1, \ldots, T \tag{9}$$

$$x_t^{B,dch,str} + x_t^{B,dch,end} \leq 1 \quad \forall t = 1, \ldots, T \tag{10}$$

$$c_t^{B,cyc} = p^{B,cyc} \cdot (x_t^{B,ch,str} + x_t^{B,dch,str}) \quad \forall t = 1, \ldots, T \tag{11}$$

In constraints (7), $x_t^{B,ch,str}$ and $x_t^{B,ch,end}$ are binary decision variables that are set to 1 at the start and end of a charging sequence respectively or 0 otherwise, while in constraints (8), $x_t^{B,dch,str}$ and $x_t^{B,dch,end}$ are binary decision variables that are set to 1 at the start and end of a discharging sequence, respectively. Constraints (9) and (10) ensure that the start and end of a charging or a discharging sequence cannot happen simultaneously. To minimize the number of charging and discharging cycles, a cycling cost $c_t^{B,cyc}$ is calculated, as reported in constraint (11), where $p^{B,cyc}$ indicates the unit cycling cost.

The relation between the active and reactive power output for BESS inverter and the size of the BESS inverter, $A^{in,B}$ provides an operating range with a circular capability curve. The CEI 0–16 standard of the Comitato Elettrotecnico Italiano (the Italian non-profit association, responsible for the technical standardization in the electrical, electronic and telecommunications fields) [50] defines the operating region of BESS inverters connected to the MV network with a capability curve as shown in Fig. 3. The relevant constraints related to the exchange of inductive reactive power are reported below.

$$0 \leq Q_t^{B,abs} \leq A^{in,B} \cdot y_t^{B,abs} \quad \forall t = 1, \ldots, T \tag{12}$$

$$0 \leq Q_t^{B,inj} \leq A^{in,B} \cdot y_t^{B,inj} \quad \forall t = 1, \ldots, T \tag{13}$$

$$y_t^{B,abs} + y_t^{B,inj} \leq 1 \quad \forall t = 1, \ldots, T \tag{14}$$

$$(P_t^{B,ch})^2 + (Q_t^{B,abs})^2 \leq (A^{in,B})^2 \quad \forall t = 1, \ldots, T \tag{15}$$

$$(P_t^{B,ch})^2 + (Q_t^{B,inj})^2 \leq (A^{in,B})^2 \quad \forall t = 1, \ldots, T \tag{16}$$

$$(P_t^{B,dch})^2 + (Q_t^{B,abs})^2 \leq (A^{in,B})^2 \quad \forall t = 1, \ldots, T \tag{17}$$

$$(P_t^{B,dch})^2 + (Q_t^{B,inj})^2 \leq (A^{in,B})^2 \quad \forall t = 1, \ldots, T \tag{18}$$

In constraints (12) and (13), $Q_t^{B,abs}$ and $Q_t^{B,inj}$ are decision variables that correspond to the inductive reactive power absorbed and supplied by the BESS inverter, respectively, while $y_t^{B,abs}$ and $y_t^{B,inj}$ are binary decision variables that are set to 1 when the BESS inverter is absorbing or supplying reactive power, respectively, or 0 otherwise. Constraint (14) prevents the simultaneous exchange of inductive and capacitive reactive power by the BESS inverter. Constraints (15)–(18) introduce nonlinearity as they describe a circular operating range. To linearize these constraints, a regular polygon is assumed to be inscribed within the circular capability curve to obtain a linearized polygonal operating range. It is assumed that the polygon has an equal number of sides H in each quadrant and the linearized constraints are reported below.

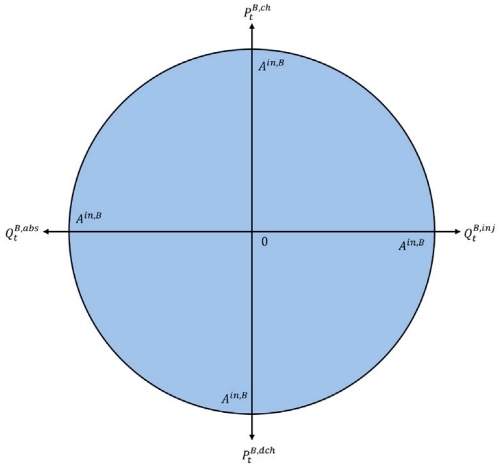

Fig. 3. Capability curve of bidirectional inverters connected to MV network.

$$P_t^{B,ch} - j_h \cdot A^{in,B} = \delta_h \cdot (Q_t^{B,abs} - i_h \cdot A^{in,B}) \quad \forall t = 1, \ldots, T \quad \forall h = 1, \ldots, H \tag{19}$$

$$P_t^{B,ch} - j_h \cdot A^{in,B} = \delta_h \cdot (Q_t^{B,inj} - i_h \cdot A^{in,B}) \quad \forall t = 1, \ldots, T \quad \forall h = 1, \ldots, H \tag{20}$$

$$P_t^{B,dch} - j_h \cdot A^{in,B} = \delta_h \cdot (Q_t^{B,abs} - i_h \cdot A^{in,B}) \quad \forall t = 1, \ldots, T \quad \forall h = 1, \ldots, H \tag{21}$$

$$P_t^{B,dch} - j_h \cdot A^{in,B} = \delta_h \cdot (Q_t^{B,inj} - i_h \cdot A^{in,B}) \quad \forall t = 1, \ldots, T \quad \forall h = 1, \ldots, H \tag{22}$$

$$i_h = A^{in,B} \cdot \cos\left((h-1) \cdot \frac{\pi}{2} \cdot \frac{1}{H}\right) \quad \forall h = 1, \ldots, H+1 \tag{23}$$

$$j_h = A^{in,B} \cdot \sin\left((h-1) \cdot \frac{\pi}{2} \cdot \frac{1}{H}\right) \quad \forall h = 1, \ldots, H+1 \tag{24}$$

$$\delta_h = \frac{j_{h+1} - j_h}{i_{h+1} - i_h} \quad \forall h = 1, \ldots, H \tag{25}$$

In constraints (19)–(25), i_h and j_h are the coordinates of the starting point of the h-th side of the polygon in the quadrant, while δ_h is the slope of the side with respect to the Cartesian plane. For a tetracontagon inscribed within the circular capability curve, it has been verified that the approximation error is less than 0.41 %.

3.1.2. Grid connection

The active power absorbed from the utility grid $P_t^{G,b}$ and the active power supplied to the utility grid $P_t^{G,s}$ are continuous decision variables limited by the size of the transformer $A^{trf,G}$ that connects the hub to the

MV network. The relevant relations related to the exchange of active power with the grid are reported in constraints (26)–(28).

$$0 \le P_t^{G,b} \le A^{trf,G} \cdot x_t^{G,b} \quad \forall t = 1, \dots, T \tag{26}$$

$$0 \le P_t^{G,s} \le A^{trf,G} \cdot x_t^{G,s} \quad \forall t = 1, \dots, T \tag{27}$$

$$x_t^{G,b} + x_t^{G,s} \le 1 \quad \forall t = 1, \dots, T \tag{28}$$

In constraints (26) and (27), $x_t^{G,b}$ and $x_t^{G,s}$ are binary decision variables that are set to 1 when the EVCH absorbs or supplies active power from/to the utility grid respectively or 0 otherwise, while constraints (28) prevent the simultaneous sale and purchase of active energy.

Constraints relating active and reactive power exchanges with the distribution network follow relations similar to the ones employed for the BESS inverter: therefore, reference is made to constraints (19)–(25).

The purchase of active energy from the public network incurs costs for the EVCH while the sale of active energy to the public network generates revenues. In order to maintain control over voltage, the injection/absorption of inductive reactive energy to/from the public network at specific time intervals attracts penalties, according to the provisions of ARERA (The Italian Regulatory Authority for Energy, Networks and Environment) [51].

$$c_t^{Grid} = \Delta \cdot \left(c_t^{Pb} \cdot P_t^{G,b} + c_t^{Q,abs} \cdot Q_t^{G,abs} + c_t^{Q,inj} \cdot Q_t^{G,inj} - r_t^{Ps} \cdot P_t^{G,s} \right) \quad \forall t = 1, \dots, T \tag{29}$$

In constraints (29), the continuous decision variables c_t^{Grid} represent the net costs related to the exchange of active and reactive energy with the network at time interval t. c_t^{Pb} and r_t^{Ps} are respectively the unitary cost related to the purchase of active energy from the network and the unitary revenue generated from the sale of active energy to the network, while $c_t^{Q,abs}$ and $c_t^{Q,inj}$ are the unitary penalties related to the absorption and injection of inductive reactive power $Q_t^{G,abs}$ and $Q_t^{G,inj}$.

3.2. RES model

3.2.1. PV power plant

The available active power from the PV power plant at each time interval, $P_t^{PV,av}$, can be obtained using the relations presented in [37,52,53], knowing the hourly incident solar irradiance data, available for the given location using the Photovoltaic Geographical Information System (PVGIS) software [54]. Constraints describing the operation of the PV plant are listed below:

$$0 \le P_t^{PV,curt} \le P_t^{PV,av} \quad \forall t = 1, \dots, T \tag{30}$$

$$P_t^{PV} = P_t^{PV,av} - P_t^{PV,curt} \quad \forall t = 1, \dots, T \tag{31}$$

$$c_t^{PV,curt} = p_t^{PV,curt} \cdot P_t^{PV,curt} \quad \forall t = 1, \dots, T \tag{32}$$

If for some reason, the active power production of the PV P_t^{PV} has to be reduced with respect to the available power $P_t^{PV,av}$, curtailed power appears $P_t^{PV,curt}$. The power that is curtailed can be at most the whole available one, as stated in (30). The actual power production of the PV is defined as in (31). The curtailment of PV active power production incurs a cost $c_t^{PV,curt}$ as indicated in constraints (32), where $p_t^{PV,curt}$ is the unit cost for PV curtailment.

P_t^{PV}, $P_t^{PV,curt}$ and $c_t^{PV,curt}$ are continuous decision variables, while $P_t^{PV,av}$ and $p^{PV,curt}$ are inputs to the model.

The relationship between the active and reactive power from the PV inverter and the size of the PV inverter provides an operating range with a semi-circular capability curve. However, the CEI 0–16 standard limits the operating region of PV inverters connected to the MV network with rated active power output below 400 kW to the blue-shaded region in Fig. 4.

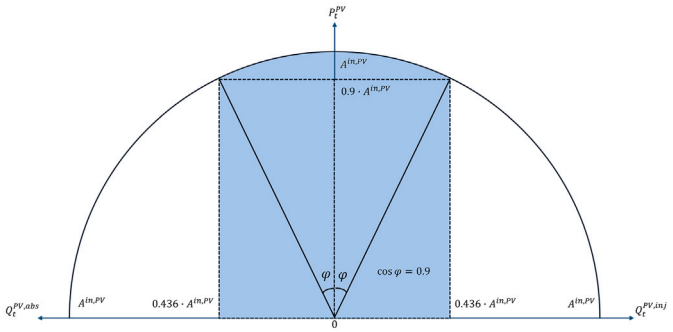

Fig. 4. Capability curve of PV inverters with rated active power output below 400 kW.

The capability curve is described by the set of constraints (33)–(34), (36)–(37), where $A^{in,PV}$ is the rating of the PV inverter.

$$0 \le Q_t^{PV,abs} \le 0.436 \cdot A^{in,PV} \cdot y_t^{PV,abs} \quad \forall t = 1, \dots, T \tag{33}$$

$$0 \le Q_t^{PV,inj} \le 0.436 \cdot A^{in,PV} \cdot y_t^{PV,inj} \quad \forall t = 1, \dots, T \tag{34}$$

$$y_t^{PV,abs} + y_t^{PV,inj} \le 1 \quad \forall t = 1, \dots, T \tag{35}$$

$$(P_t^{PV})^2 + (Q_t^{PV,abs})^2 \le (A^{in,PV})^2 \quad \forall t = 1, \dots, T \tag{36}$$

$$(P_t^{PV})^2 + (Q_t^{PV,inj})^2 \le (A^{in,PV})^2 \quad \forall t = 1, \dots, T \tag{37}$$

In constraints (33) and (34), $Q_t^{PV,abs}$ and $Q_t^{PV,inj}$ are continuous decision variables that indicate the inductive reactive power absorbed and inductive reactive power injected by the PV inverter respectively, while $y_t^{PV,abs}$ and $y_t^{PV,inj}$ are binary decision variables that are respectively set to 1 when the inverter is absorbing or injecting inductive reactive power and are set to 0 otherwise. Constraints (35) prohibit the simultaneous absorption and injection of inductive reactive power by the PV inverter. Constraints (36) and (37) describe the circular segment of the capability curve: they intrinsically introduce nonlinearity in the model, which needs to be linearized to be included in the MILP model in a similar way as carried out for the BESS capability curve.

3.2.2. Wind farm

The actual active power production for an entire year of operation of the plant is available and is used as input to the optimization model. WTs are connected to the public distribution network through full-power converters that allow the exchange of both active and reactive power. In the proposed model, a single equivalent inverter is considered for the WTs. The CEI 0–16 standard specifically limits the operation of WTs connected to the MV network with the rectangular capability curve shown in Fig. 5.

The maximum reactive power that the WT inverter can exchange is limited to 0.312 p.u. on a base power equal to the size of the WT inverter, $A^{in,WT}$. The relevant constraints are described below.

$$0 \le Q_t^{WT,abs} \le 0.312 \cdot A^{in,WT} \cdot y_t^{WT,abs} \quad \forall t = 1, \dots, T \tag{38}$$

$$0 \le Q_t^{WT,inj} \le 0.312 \cdot A^{in,WT} \cdot y_t^{WT,inj} \quad \forall t = 1, \dots, T \tag{39}$$

$$y_t^{WT,abs} + y_t^{WT,inj} \le 1 \quad \forall t = 1, \dots, T \tag{40}$$

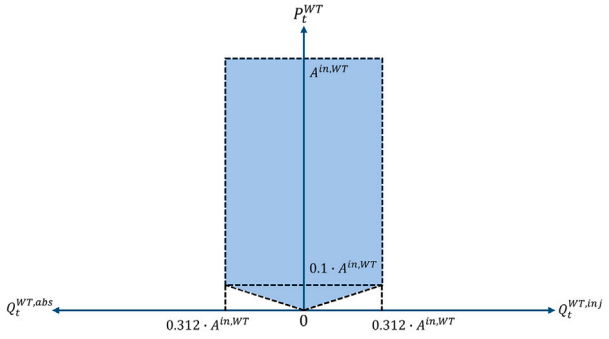

Fig. 5. Capability curve of WTs with full converters connected to MV network.

$$P_t^{WT} \geq 0.3205 \cdot Q_t^{in,abs} \quad \forall t = 1, \ldots, T \tag{41}$$

$$P_t^{WT} \geq 0.3205 \cdot Q_t^{in,inj} \quad \forall t = 1, \ldots, T \tag{42}$$

In constraints (38) and (39), limiting the reactive power exchange, $Q_t^{WT,abs}$ and $Q_t^{WT,inj}$ are decision variables that respectively correspond to the inductive reactive power absorbed and supplied by the WT inverter. The simultaneous absorption and injection of inductive reactive power by the WT inverter is avoided, as reported in constraint (40), by the use of binary decision variables $y_t^{WT,abs}$ and $y_t^{WT,inj}$, which are set to 1 when the inverter is absorbing or injecting reactive power, respectively, and are set to 0 otherwise. In constraints (41) and (42), P_t^{WT} is the active power supplied by the WT inverter: these constraints ensure that the reactive power exchanges of the WT inverter are within the operational limits, when the active power production from the WT generator is less than 0.1 p.u.

3.3. EV model

The data regarding the total active energy absorbed by the light EVs (i.e., EV cars or EV vans) utilizing the facility for an entire year of operation ($E^{EV,annual}$) has been provided by *Ricarica*, based on historical series, and used to forecast the EV demand for the following years, taking into account the projected increase in the sale of EVs, through a coefficient (α^s) dependent on the considered year. Besides, *Ricarica* provided the authors with the hourly hub usage factor of EVs (γ_t), indicating the share of the annual demand in time interval t. γ_t is based on the historical datasets of facility occupation levels, considering arrival and departure times and EV charging demands. Therefore, through Eq. (43), the total forecasted EV active power demand for each time interval $P_t^{EV,fc}$ can be determined.

The forecasted active power demand $P_t^{EV,fc}$ can be split into three contributions, which are considered as input data for the optimization problem, derived on the basis of historical data provided by *Ricarica*, as shown in (44):

- The forecasted contribution related to the EV chargers of Operator 2 $P_{w,t}^{Op_2,fc}$, where w denotes the w-th charger $(w = 1 \ldots N^{Op_2})$, with N^{Op_2} indicating the number of chargers of "*Operator* 2";
- The forecasted contribution related to "type a" EV chargers of *Ricarica* $P_{a,t}^{R_a,fc}$, where a represents the a-th charger $(a = 1 \ldots N^{R_a})$, with N^{R_a} indicating the number of chargers of "type a";
- The forecasted contribution related to "type b" EV chargers of *Ricarica* $P_{b,t}^{R_b,fc}$, where b represents the b-th charger $(b = 1 \ldots N^{R_b})$, with N^{R_b} indicating the number of chargers of "type b".

$$P_t^{EV,fc} = \left(\frac{\alpha^s \cdot \gamma_t \cdot E^{EV,annual}}{\Delta} \right) \quad \forall t = 1, \ldots, T \tag{43}$$

$$P_t^{EV,fc} = \sum_{a=1}^{N^{R_a}} P_{a,t}^{R_a,fc} + \sum_{b=1}^{N^{R_b}} P_{b,t}^{R_b,fc} + \sum_{w=1}^{N^{Op_2}} P_{w,t}^{Op_2,fc} \quad \forall t = 1, \ldots, T \tag{44}$$

The actual charging demand is supposed to be equal to the forecasted one for "type a" chargers and for the chargers of Operator 2. On the other hand, since "type b" chargers are supposed to be available for the charging of electric trucks possibly parked at the facility during the night, their actual power demand may differ from the forecasted one (which took into account only light EVs), depending on the presence of electric trucks. Therefore, the actual charging demand at the chargers of "type b" becomes a decision variable, $P_{b,t}^{R_b}$, that depends on the charging/discharging pattern of the truck.

$$P_{b,t}^{R_b} = \left(P_{b,t}^{truck,ch} - P_{b,t}^{truck,dch} \right) \cdot y_{b,t}^{truck} + P_{b,t}^{R_b,fc} \cdot \left(1 - y_{b,t}^{truck} \right) \quad \forall t = 1, \ldots, T \tag{45}$$

In constraints (45), $y_{b,t}^{truck}$ is an input data that is equal to 1 when the b-th EV truck is parked at the b-th charger at time t and 0 otherwise, supposing that each EV truck has its own dedicated charger. When EV trucks are not connected at the EVCH, the actual charging demand $P_{b,t}^{R_b}$ corresponds to the forecasted one $P_{b,t}^{R_b,fc}$, since possible light EVs are supposed to be charging in place of trucks. When the trucks are present, the charging demand is given by the difference of two continuous decision variables, $P_{b,t}^{truck,ch}$ and $P_{b,t}^{truck,dch}$, representing the charging and discharging active power of the truck connected at charger b; obviously, $P_{b,t}^{truck,dch}$ is applicable only for trucks able to perform V2G.

Finally, constraints (46) define the actual total EV net demand of the hub, P_t^{EV}, which is also a decision variable.

$$P_t^{EV} = \sum_{a=1}^{N^{R_a}} P_{a,t}^{R_a,fc} + \sum_{b=1}^{N^{Rb}} P_{b,t}^{R_b} + \sum_{w=1}^{N^{Op_2}} P_{w,t}^{Op_2,fc} \quad \forall t = 1, \ldots, T \tag{46}$$

The constraints related to the charging and discharging of the electric trucks are discussed below.

$$0 \leq P_{b,t}^{\text{truck,ch}} \leq \begin{cases} P_b^{ch,\,\max} \cdot x_{b,t}^{truck,ch} \\ \qquad \text{if } E_{b,t}^{truck} \leq 0.75 \cdot C_b^{truck} \\ P_b^{ch,\,\max} \cdot \left(1 - \frac{E_{b,t}^{truck} - 0.75 \cdot C_b^{truck}}{0.25 \cdot C_b^{truck}} \right) \cdot x_{b,t}^{truck,ch} \\ \qquad \text{if } E_{b,t}^{truck} > 0.75 \cdot C_b^{truck} \end{cases} \quad \forall b = 1, \ldots, N^{R_b}, \quad \forall t = t_b^{arr}, \ldots, t_b^{dep} \tag{47}$$

$$0 \leq P_{b,t}^{truck,dch} \leq \begin{cases} 0 \\ \qquad \text{if } E_{b,t}^{truck} \leq 0.20 \cdot C_b^{truck} \\ P_b^{dch,\,\max} \cdot \left(1 - \frac{0.50 \cdot C_b^{truck} - E_{b,t}^{truck}}{0.30 \cdot C_b^{truck}} \right) \cdot x_{b,t}^{truck,dch} \\ \qquad \text{if } 0.20 \cdot C_b^{truck} < E_{b,t}^{truck} < 0.50 \cdot C_b^{truck} \\ P_b^{dch,\,\max} \cdot x_{b,t}^{truck,dch} \\ \qquad \text{if } E_{b,t}^{truck} \geq 0.50 \cdot C_b^{truck} \end{cases} \quad \forall b = 1, \ldots, N^{R_b}, \quad \forall t = t_b^{arr}, \ldots, t_b^{dep} \tag{48}$$

$$x_{b,t}^{\text{truck,ch}} + x_{b,t}^{\text{truck,dch}} \leq y_{b,t}^{\text{truck}} \quad \forall b = 1, \ldots, N^{R_b}, \quad \forall t = t_b^{\text{arr}}, \ldots, t_b^{\text{dep}} \tag{49}$$

Main decision variables, besides of $P_{b,t}^{truck,ch}$ and $P_{b,t}^{truck,dch}$, are $x_{b,t}^{truck,ch}$ and $x_{b,t}^{truck,dch}$, which are set to 1 when the truck is charged or discharged and 0 otherwise, and the energy content of the electric truck battery, $E_{b,t}^{truck}$. Input data are the truck battery capacity C_b^{truck}, the maximum charging and discharging powers of the electric truck $P_b^{ch,\max}$ and $P_b^{dch,\max}$ and the arrival and departure time of the trucks, t_b^{arr} and t_b^{dep}; $P_b^{ch,\max}$ and $P_b^{dch,\max}$ are evaluated as the minimum between the rated

power of the charging station and the rated power of the EV truck equipment. Constraints (47) limit the charging power of the truck, depending on its energy content: when $E_{b,t}^{truck}$ exceeds a threshold (75 %), the charging power is not at its maximum but is decreased with respect to it. The same approach is followed in (48) for the discharging phase, limiting the discharging power below a certain value of $E_{b,t}^{truck}$ (50 %). Constraints (49) forbid the simultaneous charging and discharging of the EV trucks and make power exchanges possible only when trucks are present at the EVCH. Truck battery energy content constraints are presented below.

$$0.1 \cdot C_b^{truck} \leq E_{b,t_b^{arr}}^{truck} \leq 0.2 \cdot C_b^{truck} \quad \forall b = 1, \dots, N^{R_b} \tag{50}$$

$$E_{b,t_b^{dep}}^{truck} \geq 0.8 \cdot C_b^{truck} \quad \forall b = 1, \dots, N^{R_b} \tag{51}$$

$$E_{b,t+1}^{truck} = E_{b,t}^{truck} + \Delta \cdot \left(P_{b,t}^{truck,ch} \cdot \eta_b^{truck,ch} - \frac{P_{b,t}^{truck,dch}}{\eta_b^{truck,dch}} \right) \quad \forall b = 1, \dots, N^{R_b} \quad \forall t = t_b^{arr}, \dots, t_b^{dep} - 1 \tag{52}$$

$$SoC_b^{\text{truck,min}} \cdot C_b^{\text{truck}} \leq E_{b,t}^{\text{truck}} \leq SoC_b^{\text{truck,max}} \cdot C_b^{\text{truck}} \quad \forall b = 1, \dots, N^{R_b} \quad \forall t = t_b^{arr}, \dots, t_b^{dep} \tag{53}$$

In constraints (50), the energy content of the electric truck at its time of arrival is assumed to be within an interval close to the minimum energy content. Constraints (51) state that the energy content of the electric truck has to be above or equal to 80 % of the rated capacity at its time of departure. The energy balance of the truck is expressed by (52), where $\eta_b^{truck,ch}$ and $\eta_b^{truck,dch}$ are the charging and discharging efficiencies. The energy content of the truck has to be limited between a minimum and a maximum value as stated by (53), where $SoC_t^{truck,\min}$ and $SoC_t^{truck,\max}$ are the minimum and maximum SoCs for the truck connected to charger b.

A penalty, $Penalty_{b,t_b^{dep}}^{truck}$, is levied on the EVCH if the EMS can't ensure that the truck battery is charged to the maximum allowable SoC at the time of departure. $Penalty_{b,t_b^{dep}}^{truck}$ is a decision variable function of the energy content of the EV truck at the time of departure: indeed, it increases as the difference ($Diff_{b,t_b^{dep}}^{truck}$) between the maximum energy content of the truck battery and the final energy content of the truck at departure time, as described in (54).

$$Diff_{b,t_b^{dep}}^{truck} = SoC_b^{truck,\ \max} \cdot C_b^{truck} - E_{b,t_b^{dep}}^{truck} \quad \forall b = 1, \dots, N^{R_b} \tag{54}$$

Although the overnight charging of trucks attracts revenues to the hub, the discharging of the electric truck batteries leads to additional costs for the EVCH, since V2G service has to be remunerated to the owners of the trucks. The net costs $c_{b,t}^{truck}$ related to the charging of the b-th electric truck are expressed in (55).

$$c_{b,t}^{truck} = \Delta \cdot \left(p^{truck,dch} \cdot P_{b,t}^{truck,dch} - r^{truck,ch} \cdot P_{b,t}^{truck,ch} \right) \quad \forall b = 1, \dots, N^{R_b} \quad \forall t = t_b^{\text{arr}}, \dots, t_b^{\text{dep}} \tag{55}$$

where $p^{truck,dch}$ is the unitary remuneration for the provision of V2G service, paid to the owner of the truck by *Ricarica*, and $r^{truck,ch}$ is the charging fee, paid by the truck owner to *Ricarica*.

3.4. Electric power balances

The active power demand of the building and of the EVs charging at the facility and the reactive power demand of the building need to be satisfied at all time intervals. The constraints related to the electric active and reactive power balances of the hub are reported in (56) and (57).

$$P_t^{El} + P_t^{EV} + P_t^{B,ch} + P_t^{G,s} = P_t^{G,b} + P_t^{B,dch} + P_t^{W} + P_t^{PV} \quad \forall t = 1, \dots, T \tag{56}$$

$$Q_t^{El} + Q_t^{G,inj} + Q_t^{B,abs} + Q_t^{PV,abs} + Q_t^{WT,abs} = Q_t^{G,abs} + Q_t^{B,inj} + Q_t^{WT,inj} + Q_t^{PV,inj} \quad \forall t = 1, \dots, T \tag{57}$$

where P_t^{El} and Q_t^{El} are the active and reactive power demands of the building.

3.5. Objective function

The objective of the EMS is to minimize the net daily operating costs of the hub to be sustained by *Ricarica*. They include:

- the net costs related to the exchange of active and reactive power with the distribution grid;
- the costs related to the curtailment of PV;
- the cycling costs of the BESS;
- the net costs incurred due to the overnight charging of electric trucks at the facility, related to smart charging and V2G services;
- the penalty incurred due to the unsatisfied charging demand of electric trucks;
- the penalty related to peak power absorption from the utility grid.

The objective function is formulated as described in (58).

$$Obj = \sum_{t=1}^{T} \left(c_t^{PV,curt} + c_t^{B,cyc} + c_t^{Grid} + \sum_{b=1}^{N^{Rb}} c_{b,t}^{truck} \right) + \sum_{b=1}^{N^{Rb}} Penalty_{v,t_b^{dep}}^{truck} + Penalty^{G,\max} \tag{58}$$

where $Penalty^{G,\max}$ is the penalty incurred by the EVCH regarding the absorption of active power from the utility grid: it is given by the product of a unit tariff, defined by the distribution system operator, and of the maximum absorption of active power from the grid in the examined period. This penalty is applied according to Italian grid codes in order to reduce grid congestion.

4. Results

The results of optimization are discussed in this section after a brief description about the input data used in the optimization model.

4.1. Input data

The input data used in the optimization model are presented in the sections below and they mainly refer to the proposed technologies (PV, WT, BESS and EV chargers).

4.1.1. General input data

The optimization horizon is 1 week ($T = 168$) with a time interval duration Δ of 1 hour.

4.1.2. PV model

The size of the PV inverter $\left(A^{in,PV}\right)$ is 0.39 [MVA] while the unit cost of PV curtailment is 0.128 [€/kWh] [55]. The PV plant is made up of 588 modules, installed on the building rooftop, with three different orientations and tilt angles, in order to exploit all the available surface.

4.1.3. Wind farm

The size of the WT inverter $\left(A^{in,WT}\right)$ is 9.4 [MVA] and the peak active power production from the WT farm from yearly measured data is 8.78 [MW].

4.1.4. BESS

The size of the BESS inverter $\left(A^{in,B}\right)$ has been optimally designed to 0.335 [MVA]. The BESS has a rated capacity of 1.488 [MWh] with charging and discharging efficiencies assumed respectively equal to 97 [%]. The minimum, maximum and initial SoCs are respectively equal to 20 [%], 100 [%] and 20 [%], while the self-discharge rate is assumed to be 0 [-].

4.1.5. MV distribution network

The size of the transformer $A^{trf,G}$ which connects the EVCH to the MV distribution network is 12 [MVA]. The electricity purchase price c_t^{Pb} is set equal to the zonal market clearing price, with an addition of 0.08 [€/kWh] while the electricity selling price r_t^{Ps} is set at the zonal market clearing price. The unit penalty for the absorption and injection of reactive power from the utility grid, $c_t^{Q,abs}$ and $c_t^{Q,inj}$, are set to 0.00606 [€/kVArh] and 0.00456 [€/kVArh]. The penalty for inductive reactive power absorption is only applicable during F1 and F2 time slots while the penalty on the inductive reactive power injection is applicable during the F3 time slot, as defined by ARERA.

4.1.6. EV

The total number of "*type a*" EV chargers is 2, with a rated power of 350 [kW] for each charger, while the total number of "*type b*" EV chargers is 1, with a rated power of 75 [kW]. The number of EV chargers of Operator 2 is 12, each one characterized by a rated power of 250 [kW]. Only one electric truck is considered. It is present at the EVCH overnight, from 8 pm until 8 am, from Monday evening to Saturday morning. It is not present on weekends. The electric truck has a rated battery capacity of 450 [kWh]. The electric truck battery is to be maintained between a minimum SoC of 10 % and a maximum SoC of 98 %. Considering quick charging, the maximum active power that can be charged to the truck, $P^{ch,\max}$ is 75 [kW], while the maximum active power that can be discharged by the truck, $P^{dch,\max}$ is 50 [kW]. These values are increased up to 250 [kW] in case of fast charging. The values of the charging fee $r^{truck,ch}$ and of the V2G service remuneration $p^{truck,dch}$ are set equal to 0.58 [€/kWh] and 0.35 [€/kWh] respectively. The former has been set equal to the average EV quick/fast charging fee and the latter has been defined in accordance with the one proposed in [56].

4.2. Optimization results

The model was implemented in Matlab R2022b environment with the help of Yalmip [57] and solved using the Gurobi solver [58]. To explore the effectiveness of the EMS, two base scenarios are analysed: in the first one (Scenario I), V2G is considered along with the BESS, while the second one (Scenario II) considers the provision of V2G services with the BESS being out of service. For both scenarios, a unique summer week of operation is studied. Further scenarios will be analysed through the sensitivity analyses described in Section 4.2.4.

The active and reactive energy demand of the EVCH is equal for both Scenario 1 and Scenario 2: the same applies to the active energy production from the PV and WT plants. Fig. 6 presents the total electric demand at the EVCH split into active power demand of the building, forecasted EV active power demand and reactive power demand of the building. In these plots, as well as in the following ones, the first considered day is Friday.

Similarly, the active power production from the PV power plant and the WT farm for the considered week of operation are presented in Fig. 7.

The hourly unit cost and revenue related to the purchase and sale of active energy are presented in Fig. 8.

4.2.1. Scenario I: EVCH operation with electric truck in V2G mode

In this scenario, the electric truck parked at the facility is also allowed to discharge its battery by exploiting the V2G functionality. Fig. 9 presents the BESS discharging power and the power withdrawn from the distribution network, while Fig. 10 shows the BESS charging power and the power injected into the distribution network.

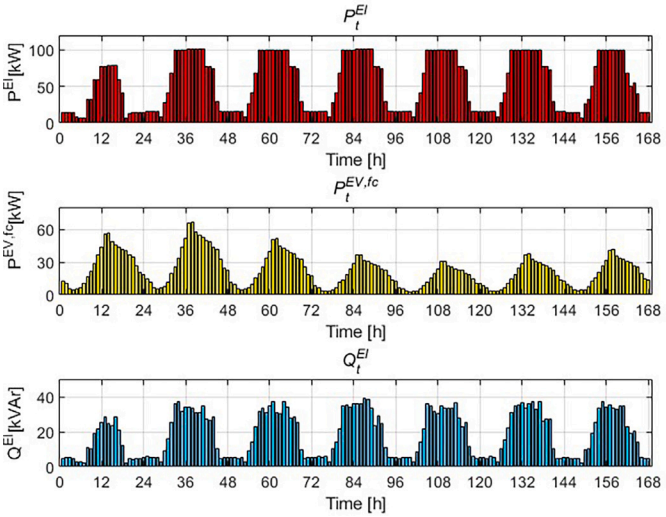

Fig. 6. Electric load demands at the EVCH.

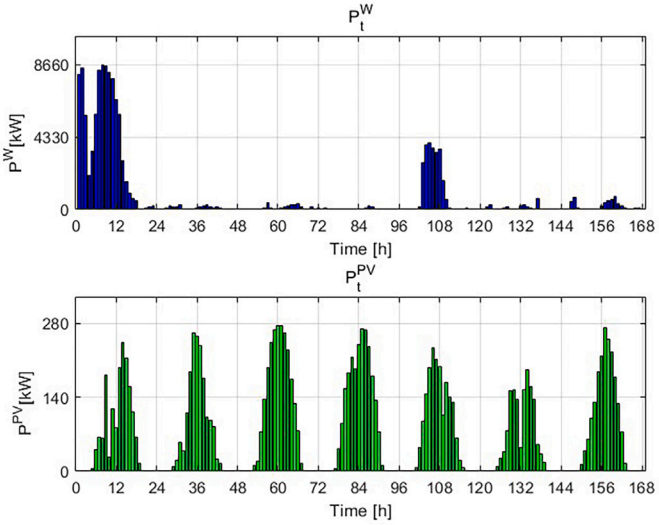

Fig. 7. Active power production from the WT farm and PV system.

During the considered week, no active energy is purchased from the utility grid, since the RES power plants along with the BESS are able to satisfy the energy demand of the hub on their own. Besides, BESS is used to absorb possible excess RES production (thus avoiding curtailment of PV) and to perform peak shaving, reducing the peak power withdrawn from the network and the relevant penalty. During days of large WT production, the active energy sold to the network reaches relevant values.

The operation of the EMS can be studied in detail by considering the active power balance on a day with low active energy output from the WT farm. The active power balance for such a day is presented in Fig. 11.

It can be seen that the BESS is charged when the active power output from the WT farm and the PV system is in excess with respect to the load; BESS is later discharged when the selling price for active energy reaches a daily peak, to reduce the net costs of the EVCH.

In addition, the BESS is used to satisfy the load demand when there is no active energy output from the RESs. Moreover, it can be noted that there are no unnecessary charge and discharge half-cycles, thanks to the inclusion of the constraints related to the cycling of the BESS.

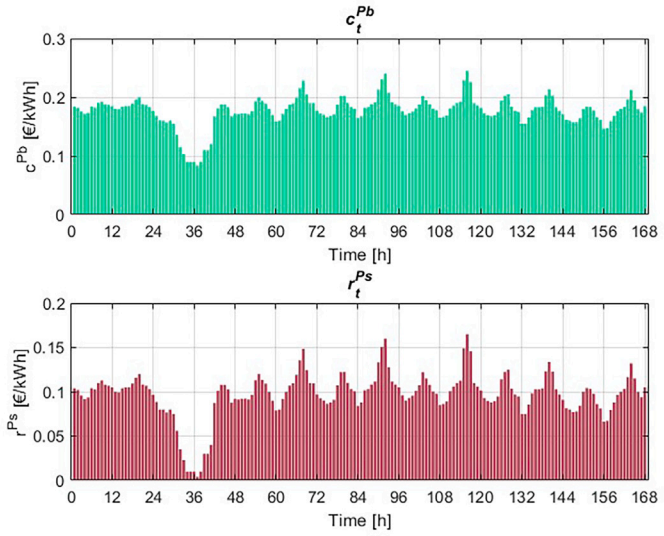

Fig. 8. Unit cost and revenue related to exchange of active energy with the distribution network.

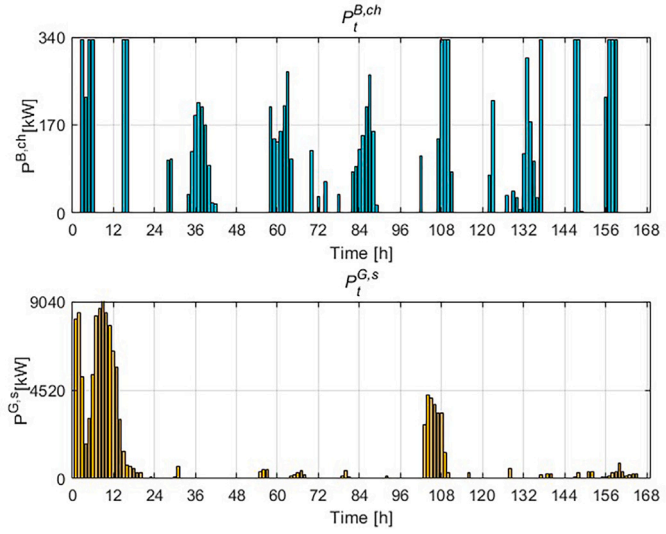

Fig. 10. BESS charging power and power injected into the distribution network in Scenario I.

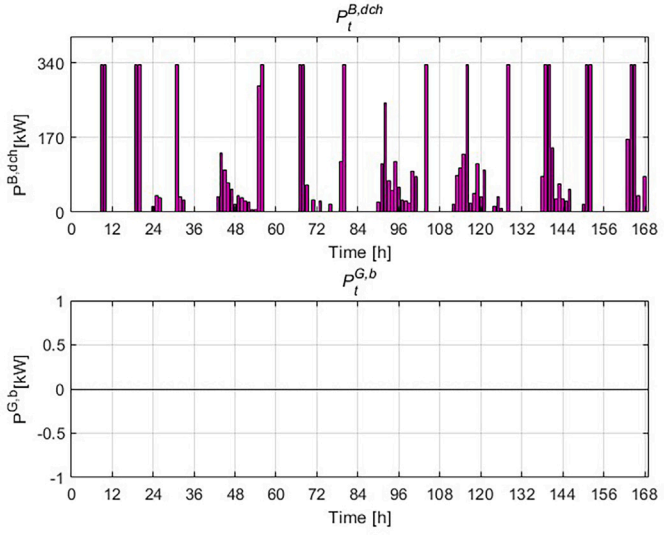

Fig. 9. BESS discharging power and power withdrawn from the distribution network in Scenario I.

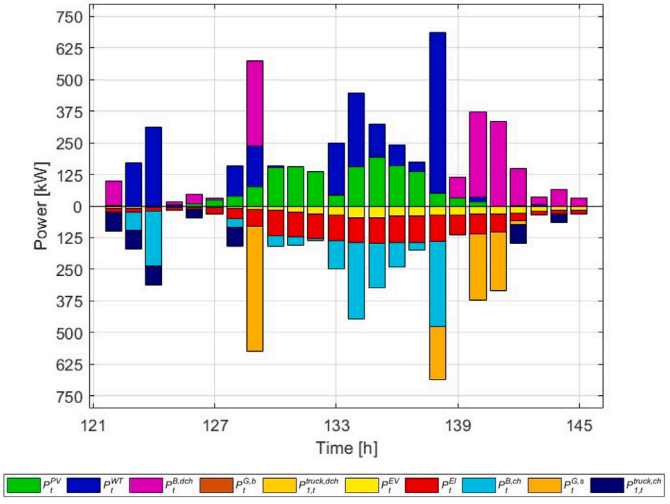

Fig. 11. Active power balance on a day with low active power production from WT farm in Scenario I.

The operation of the BESS in this scenario is presented in Fig. 12, showing that BESS is well exploited throughout the week to perform peak shaving and increase revenues.

The operation of the electric truck is shown in Fig. 13. It is charged overnight at the hub and the charging rate varies according to the SoC of its battery. At times of low active power output from the WTs, V2G is exploited, with the truck battery being discharged. Since the BESS is in operation, the truck battery is not used continuously and V2G is only exploited at certain time intervals when the active energy output from the WT farm is null.

The reactive energy balance for the hub is presented in Fig. 14, showing that the PV and WT inverters oversee satisfying the relevant demand. One inverter, at a time, is able to satisfy the demand, due to the limited reactive power load. Moreover, to avoid any penalties, no inductive reactive power is absorbed from or injected into the utility grid. The operating points of the PV and WT inverters within their capability curves are presented in Figs. 15 and 16 respectively. All the points lay within the portion of curves prescribed by CEI 0–16 standard.

4.2.2. Scenario II: EVCH operation with electric truck in V2G mode and BESS out of service

In this scenario, the BESS is assumed to be out of service for the whole week. The active power exchanges with the external network are presented in Figs. 17 and 18. Since the BESS is not in service, the active energy absorption from the utility grid has increased to satisfy the load demand. The maximum peak absorption has increased too, incurring in higher penalties.

The active power balance on a day with low active power production from the WT farm is shown in Fig. 19. It can be seen that at times when the WT farm is unable to satisfy the load demand, active energy is absorbed from the utility grid, along with the discharging of the electric truck battery to satisfy the load demand. Excess active energy output is almost always injected into the network due to lack of BESS. A portion is stored in the electric truck to be then exploited through V2G.

The charging and discharging of the electric truck over the whole week are shown in Fig. 20. Due to the unavailability of the BESS, the presence of the truck is more beneficial in this scenario than in the first

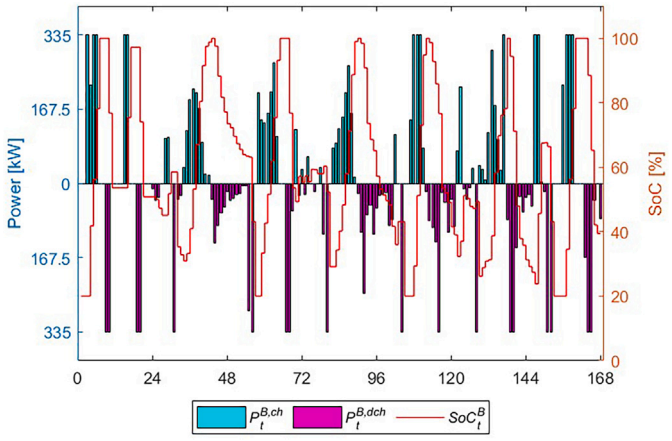

Fig. 12. BESS operation in Scenario I.

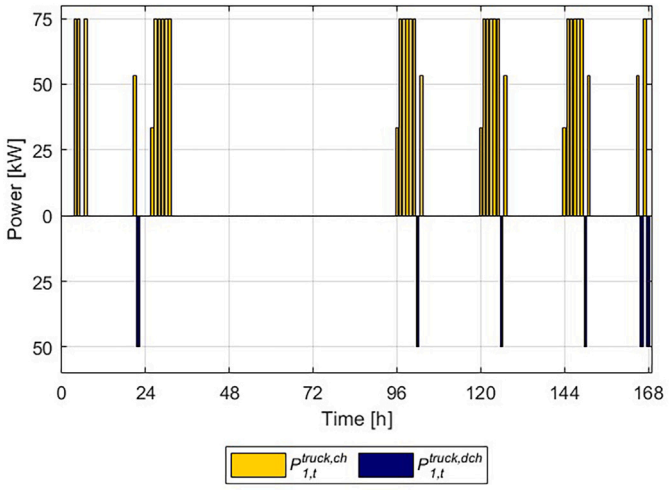

Fig. 13. Charge and discharge patterns for the electric truck in Scenario I.

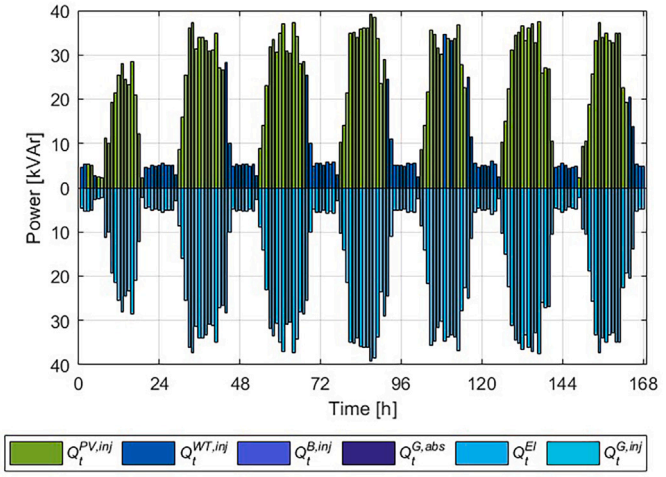

Fig. 14. Reactive power balance in Scenario I.

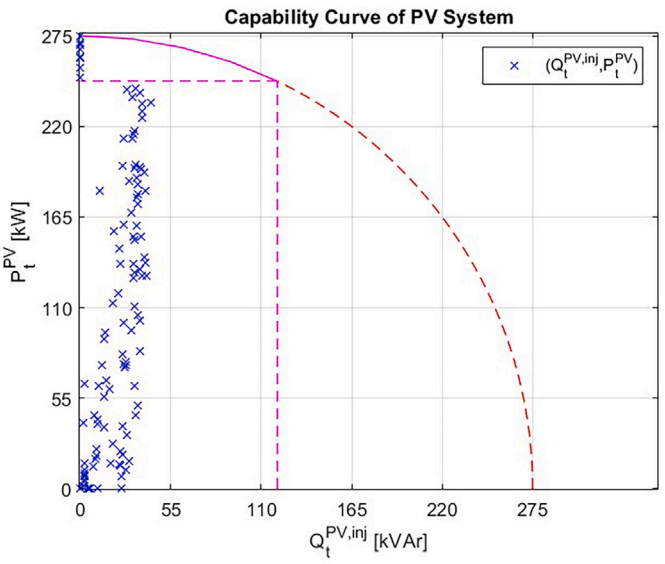

Fig. 15. Capability curve of PV plant.

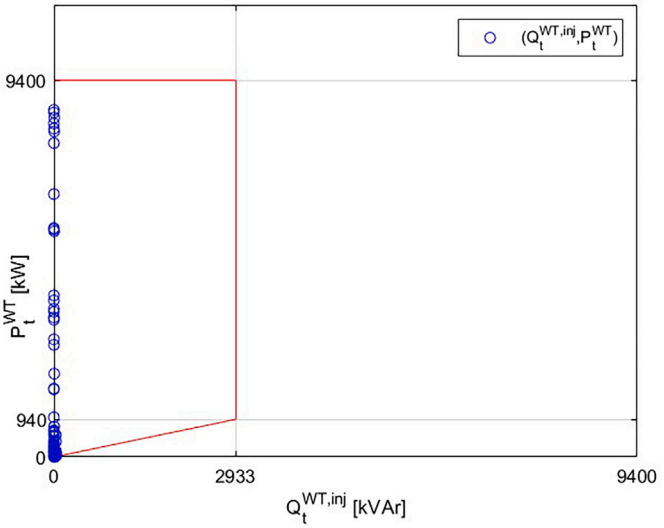

Fig. 16. Capability curve of WTs.

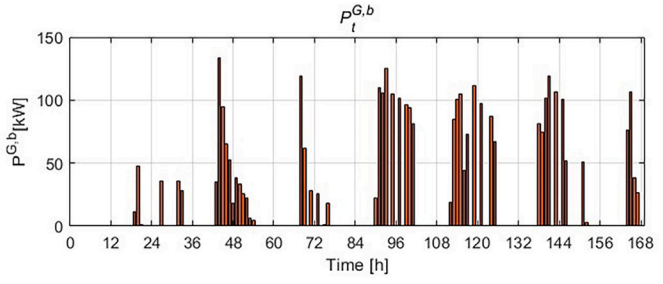

Fig. 17. Active power withdrawn from the distribution network in Scenario II.

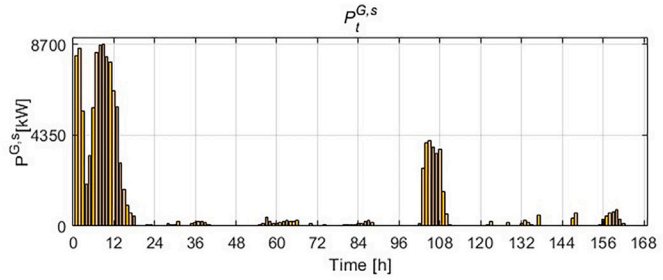

Fig. 18. Active power injected into the distribution network in Scenario II.

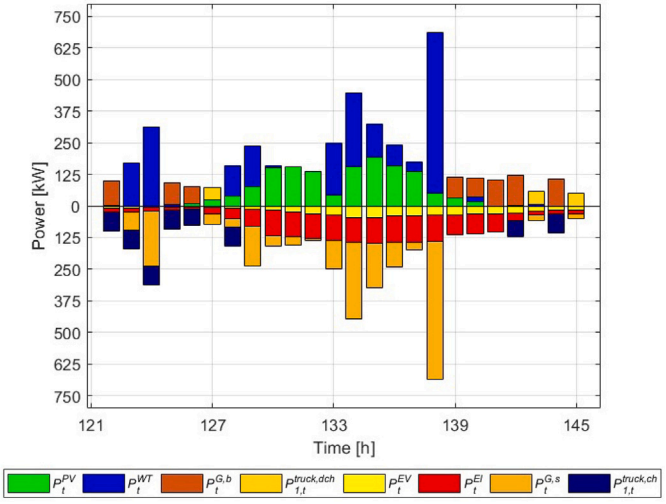

Fig. 19. Active power balance on a day with low active power production from WT farm in Scenario II.

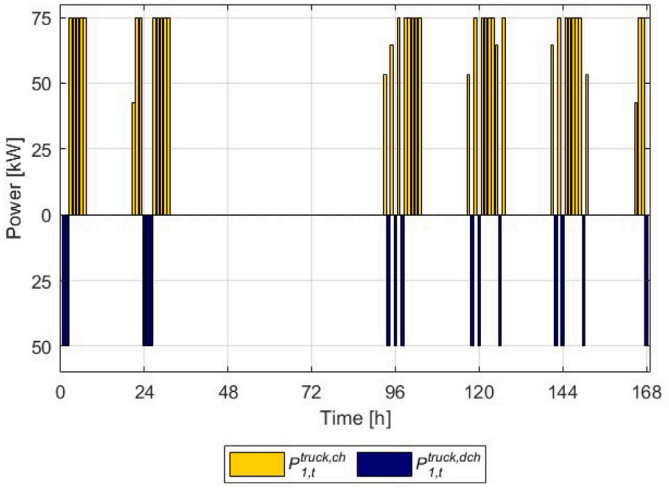

Fig. 20. Charging and discharging patterns for the electric truck in Scenario II.

one, since V2G is exploited for longer periods of time in order to avoid the withdrawal of power from the external network.

The charging and discharging patterns of the EV truck from Wednesday evening to Thursday morning are reported in Fig. 21, which also shows the SoC trend of the truck battery. In order to avoid penalties, the SoC at the departure time is the desired one, i.e., the maximum.

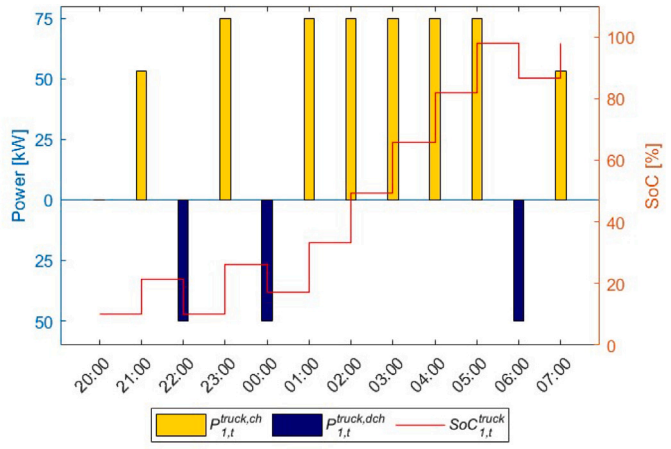

Fig. 21. Charging and discharging patterns and SoC trend for EV truck, from Wednesday evening to Thursday morning.

Table 2
Optimal values of active energy quantities.

[MWh]	Scenario	
	I	II
$E^{El,P}$	9.28	9.28
E^{EV}	6.21	6.21
$E^{PV,P}$	12.98	12.98
$E^{WT,P}$	131.68	131.68
$E^{G,b,P}$	0	3.52
$E^{G,s,P}$	126.25	130.59
$E^{B,dch}$	9.60	–
$E^{B,ch}$	10.42	–
$E^{truck,dch}$	0.30	0.75
$E^{truck,ch}$	2.20	2.83

Charging and discharging phases are defined by the need to minimize the net operating costs of the EVCH.

The reactive energy balance for the hub in Scenario II is similar to that of Scenario I, presented in Fig. 14, where the RES inverters completely satisfy the reactive power demand to avoid incurring any penalties. The same applies to the capability curve plots.

4.2.3. Comparative analysis

The active energy quantities of the optimization results for Scenario I and Scenario II are presented in Table 2. $E^{El,P}$ and E^{EV} respectively represent the weekly active energy demand of the building and of the EVs. For both Scenario I and II, the share of active energy output from the PV plant and the WT farm ($E^{PV,P}$ and $E^{WT,P}$ respectively) are constant. Since the two scenarios differ in the use of the BESS, Scenario II has a larger amount of active energy purchased from the public grid ($E^{G,b,P}$) and also overcomes Scenario I in the sale of excess active energy ($E^{G,s,P}$) to the public grid, due to the fact that excess production cannot be stored when the truck is not available but has to be sold. The BESS charged ($E^{B,ch}$) and discharged ($E^{B,dch}$) active energy quantities are applicable only to Scenario I. Scenario II utilizes the V2G capability efficiently as the active energy charged to the electric truck battery, $E^{truck,ch}$, has a higher value in scenario II as the active energy discharged by the electric truck battery $E^{truck,dch}$ increases. To further examine the impact of BESS availability, the facility's normalized operating costs reported in Table 3 are analysed. In Table 3, to normalize the quantities, the corresponding operating costs in Scenario I have been used as the base value.

From Table 3, it can be seen that the absence of the BESS impacts the operating costs due to the additional energy purchased from the public network at intervals when the wind farm is not in operation. Therein, $c_I^{B,cyc}$ represents the BESS cycling cost in Scenario I and c_I^{Grid} represents

Table 3
Optimal values of economic quantities.

	Scenario	
	I	II
$c^{PV,curt}$	0	0
$c^{B,cyc}$	$c_I^{B,cyc}$	–
c^{Grid}	c_I^{Grid}	+3.6 %
$Penalty^{truck}$	0	0
$Penalty^{G,\max}$	0	$Pe_{II}^{G,\max}$

Table 4
Comparison of EVCH cost performance when applying V0G, V1G and V2G to the electric truck.

	Scenario		
	II-V2G	II-V1G	II-V0G
$c^{PV,curt}$	0	0	0
c^{Grid}	+3.6 %	+6.2 %	+13.3 %
$Penalty^{truck}$	0	0	0
$Penalty^{G,\max}$	$Pe_{II}^{G,\max}$	+2.1 %	+3.4 %

the total net costs related to active and reactive power exchange with the external network in Scenario I. Since in Scenario I no active power is purchased from the network, the penalty on the peak absorption is equal to 0, thus the "base" quantity for the sensitivity analyses carried out in the following is the peak penalty absorption in Scenario II, $Pe_{II}^{G,\max}$.

To further demonstrate the effectiveness of the proposed charging strategy, the normalized economic results from Scenario II are compared with those that would be obtained by implementing smart charging (V1G) and traditional charging (V0G) for the electric truck. In smart charging, the charging process is optimized to minimize operating costs by varying the charging power, whereas in traditional charging, the truck is charged continuously from arrival to departure at the minimum power required to meet its energy demand. The comparison results are presented in Table 4.

From Table 4, it is evident that the application of V2G to the electric truck yields higher revenues compared to other charging approaches: indeed, since in the Scenario II the BESS is out of service, V2G-enabled truck allows to store RES production and to exploit possible electricity price fluctuations, leading to a reduction in the EVCH operating costs. Moreover, V2G-enabled truck also enhances the independence of the EVCH from the external distribution grid.

4.2.4. Sensitivity analysis

Key factors influencing the operation of the EMS include truck availability and the purchase price of electricity. To analyze their impact, Scenario II is optimized under different operating conditions to provide an insight into their impact on the facility's operating costs. The different cases are as follows: Scenario II-A: operation with high electricity purchase prices; Scenario II-B: operation with truck present at the facility during the day; Scenario II-C: operation with both high electricity prices and truck at the facility during the day. In the aforementioned scenarios, the RES production is kept constant with respect to Scenario I and Scenario II. As in Scenario II, the BESS is considered out of service. Moreover, quick charging is considered (i.e., $P_b^{ch,\max}$ equal to 75 [kW] and $P_b^{dch,\max}$ equal to 50 [kW]. The optimal results of these simulations are summarized in Table 5.

From Table 5, it can be noted that as the electricity purchase prices increase, the amount of active energy purchased from the network is reduced drastically. Also, with the increase in electricity purchase prices, an increase in the active energy discharged by the truck can be noted: indeed, V2G is exploited to supply power to the local loads. However, with the truck present during the central hours of the day, the need for the V2G capability of the truck is minimal, given that the WTs and the peak PV production meet the active energy demand.

Table 5
Optimal energy results for Scenario II subcases -High RES production.

[MWh]	Scenario			
	II	II-A	II-B	II-C
$E^{El,P}$	9.28	9.28	9.28	9.28
E^{EV}	6.21	6.21	6.21	6.21
$E^{PV,P}$	12.98	12.98	12.98	12.98
$E^{WT,P}$	131.68	131.68	131.68	131.68
$E^{G,b,P}$	3.52	3.43	2.75	2.78
$E^{G,s,P}$	130.59	130.59	129.67	129.71
$E^{truck,dch}$	0.75	0.80	0.00	0.01
$E^{truck,ch}$	2.83	2.80	2.27	2.28

Table 6
Optimal energy results for Scenario II subcases - Low RES production.

[MWh]	Scenario			
	II-D	II-E	II-F	II-G
$E^{El,P}$	9.23	9.23	9.23	9.23
E^{EV}	3.83	3.83	3.83	3.83
$E^{PV,P}$	9.95	9.95	9.95	9.95
$E^{WT,P}$	32.98	32.98	32.98	32.98
$E^{G,b,P}$	3.14	3.13	2.83	2.83
$E^{G,s,P}$	30.94	30.93	30.46	30.46
$E^{truck,dch}$	0.35	0.35	0	0
$E^{truck,ch}$	2.42	2.42	2.27	2.27

Another important aspect of the EMS to be explored is the facility's operation during periods of low active energy output from WTs. To investigate this, an additional set of simulations is conducted to analyze the facility's performance with the BESS out of service during a week of reduced wind energy generation. The case studies that examine the facility's performance under these conditions are as follows: Scenario II-D: operation under low active energy production (same electricity prices as Scenario II and nighttime truck availability); Scenario II-E: operation under low active energy production and high electricity purchase prices; Scenario II-F: operation under low active energy production and truck present during the day; Scenario II-G: operation under low active energy production with both high electricity prices and daytime truck availability. In all the aforementioned Scenario II subcases, quick charging for the electric truck is considered. The results of these analyses are summarized in Table 6.

In Table 6, it can be noted that an increase in the electricity prices does not correspond to a significant reduction in the energy purchased from the network. Indeed, given the reduced RES availability, it happens that the load must necessarily be met by withdrawing electricity from the distribution network. In Scenarios II-D and II-E, the energy exchanged between truck and EVCH is reduced with respect to Scenarios II and II-A, due again to the low availability of RES energy. As for Scenarios II-B and II-C, also in Scenarios II-F and II-G the V2G capability of the electric truck remains unused when the truck is present at the facility during the central hours of the day, as RES generation is sufficient to meet the active energy demand. Thus, in case of reduced RES production, increased electricity prices do not have a significant impact on the power exchange with the external network: on the other hand, this impact is visible when varying the presence of the truck at the EVCH. A summary of the total costs and total revenues for all the Scenario II simulation studies is presented in Table 7.

From Table 7, in all the scenarios, the effect of varying the parameters has an impact on the EVCH's operating costs. The largest net cost increase is evident in the subcases when the RES production is reduced, reaching percentages around +80 %. The impact of the time of presence of the truck at the facility is more limited than the impact of the RES production: nevertheless, daytime availability of the truck nullifies the V2G contribution, thus contributing to an increase in the overall costs. For

Table 7
Operating costs of Scenario II subcases under quick charging.

	Scenario							
	II	II-A	II-B	II-C	II-D	II-E	II-F	II-G
$c^{PV,curt}$	0	0	0	0	0	0	0	0
c^{Grid}	+3.6 %	+5.9 %	+3.1 %	+5.2 %	+78 %	+80 %	+78 %	+80 %
$Penalty^{truck}$	0	0	0	0	0	0	0	0
$Penalty^{G,\max}$	$Pe_{II}^{G,\max}$	+2.2 %	+1.7 %	+2.7 %	+0.7 %	+0.9 %	+1.1 %	+1.4 %

Table 8
Optimal energy results for Scenario II subcases.

[MWh]	Scenario							
	II	II-A	II-B	II-C	II-D	II-E	II-F	II-G
$E^{El,P}$	9.28	9.28	9.28	9.28	9.23	9.23	9.23	9.23
E^{EV}	6.21	6.21	6.21	6.21	3.83	3.83	3.83	3.83
$E^{PV,P}$	12.98	12.98	12.98	12.98	9.95	9.95	9.95	9.95
$E^{WT,P}$	131.68	131.68	131.68	131.68	32.98	32.98	32.98	32.98
$E^{G,b,P}$	2.63	2.63	2.68	2.68	3.18	3.18	2.81	2.81
$E^{G,s,P}$	129.61	129.61	129.73	129.73	30.95	30.95	30.51	30.51
$E^{truck,dch}$	0.79	0.79	0	0	1.58	1.58	0	0
$E^{truck,ch}$	2.97	2.97	2.27	2.27	3.72	3.72	2.27	2.27

Table 9
Operating costs of Scenario II under fast charging.

	Scenario							
	II	II-A	II-B	II-C	II-D	II-E	II-F	II-G
$c^{PV,curt}$	0	0	0	0	0	0	0	0
c^{Grid}	+3.1 %	+5.1 %	+2.9 %	+4.9 %	+77.5 %	+79.4 %	+77.8 %	+79.7 %
$Penalty^{truck}$	0	0	0	0	0	0	0	0
$Penalty^{G,\max}$	+1.2 %	+2.1 %	+1.57 %	+2.43 %	+0.65 %	+0.79 %	+1.46 %	+1.27 %

confidentiality reasons, the economic results are normalized on the basis of the corresponding ones obtained for Scenario I, with the exception of the increase in the penalty for peak power absorption that is compared with the one incurred by the EVCH in Scenario II, $Pe_{II}^{G,\max}$, since in Scenario I that value was equal to 0, since no power was withdrawn from the distribution network.

To provide a further insight, the operation of the facility under Scenario II is further explored by utilizing the fast charger to be used for overnight charging of the electric truck (i.e., maximum rated charging and discharging power set at 350 [kW]). The optimal results of this analysis are presented in Table 8.

In Table 8, the EVCH's operation resembles that of the analyses involving quick charging; however, a noticeable reduction in active energy absorbed from the external network is observed.

The normalized operating costs for fast charging cases are presented in Table 9. The increase in the penalty for peak absorption is provided with respect to $Pe_{II}^{G,\max}$.

From Table 9, in the fast charging cases, the operating costs of the EVCH are slightly improved compared to those of the quick charging simulation studies due to fewer charging intervals.

4.3. Validation

In order to further validate the effectiveness of the model, an optimization was performed in HOMER Grid [59] implementing the technologies present at the EVCH. The same input data has been used for the analysis. HOMER Grid does not allow to implement V2G technology, thus only smart charging is applied. The scenario that has been implemented is Scenario II, as described in Section 4.2.2. The proposed EMS has been run over one year, to be able to compare the results with the ones obtained by HOMER Grid. The main results are shown in Table 10.

From Table 10, it can be noted that results of the EMS model presented in this paper and the results of HOMER Grid are similar, thus

Table 10
Comparison between EMS and HOMER grid.

	EMS	HOMER grid
$E^{G,b,P}$	96.240 MWh	100.76 MWh
$E^{G,s,P}$	19,116 MWh	19,108 MWh
$E^{truck,ch}$	145.44 MWh	64.343 MWh
c^{Grid}	c_{EMS}^{Grid}	+6.35 %

further validating the effectiveness of the proposed model. Since the proposed EMS is able to exploit the V2G capability of the electric truck, the energy costs incurred by EVCH in HOMER Grid optimization are increased by 6.35 % with respect to the one obtained by the authors. Indeed, it is evident that the energy that is charged into the electric truck is much larger in the case of the proposed EMS, since it is used not only to satisfy the transportation demand but also for V2G. Moreover, a reduction in the energy that is withdrawn from the network and an increase in the energy injection into the network are evident from the optimal results of the proposed EMS, compared to those of HOMER Grid.

5. Conclusions

The coupling of electric mobility and RESs will represent a key solution in reducing GHG emissions. Effective management of EVCHs with locally produced renewable energy will play a significant role, due to the complexity of integrated EV-RES systems: the adoption of BESSs and the implementation of smart charging strategies thanks to their flexibility present a solution to smooth RES fluctuations and to reduce distribution network congestion.

To foster the aforesaid considerations, the present study has described an EMS for a real EVCH, owned by *Ricarica* company (a division of *Fera* group), located in Italy, able to host also electric trucks. The EVCH is coupled to large-scale RES power plants (a PV plant on the

rooftop of a building and a WT farm, connected to the EVCH through a dedicated line), in addition to a BESS. The EMS has to minimize the net operating costs of the facility, related to the exchange of active and reactive power with the distribution network, as well as to the provision of charging services through the EV charging infrastructure, like V2G applied to electric trucks. Cycling aging of BESS has also been considered. Real data about EV charging demand and WT production have been provided by *Fera* and *Ricarica* to the authors. A smart management of the EVCH allows the facility to be almost independent from the network, thus reducing emissions and providing a sustainable charging service to EV owners.

The validation of the EMS with respect to HOMER Grid has been successful, highlighting the better performance of the proposed model, thanks to the application of V2G. The profitability of V2G with respect to V0G and V1G has been proved, showing that in the absence of the BESS, V1G and V0G would induce a +6.2 % or +13.3 % increase in the net costs with respect to the net costs incurred by the EVCH in case of V2G-enabled truck.

Nine scenarios have been analysed, to evaluate the impact of V2G under different operating conditions (i.e., high/low energy availability by WTs and PV, daytime/nighttime availability of the truck at the EVCH, high/low electricity prices): the sensitivity analyses proved that V2G is beneficial, especially in situations where the BESS is out of service. Indeed, considering a high RES production, V2G allows to keep the cost increase limited to +3.6 % in case of BESS failure. Under the same RES production scenario, high electricity prices increase the overall net operating costs of the facility by +5.9 % but induce a larger exploitation of V2G (+0.05 MWh over the considered week). Finally, daytime availability of the truck limits the possibility of exploiting V2G, since the availability of the truck would coincide with the peak production by WT and PV plants. Scenarios with low RES production are characterized by a limited use of V2G, compared to scenarios with high RES availability, since a smaller excess of production with respect to the load is available. Again, daytime availability prevents the exploitation of V2G.

Regarding possible limitations of the study, battery degradation is one of the areas of possible improvement of the model: indeed, due to the reduced considered time horizon, truck battery degradation has been ignored, while BESS degradation was accounted for through a cost term in the objective function penalizing the overall number of cycles. Moreover, the impact of a single truck on the facility operation is limited (e.g., around 2 % of the energy demand in Scenario II), while the impact of a fleet of electric trucks should be investigated: indeed, a larger truck fleet might involve a higher exploitation of V2G, counterbalanced by higher battery degradation costs. Consequently, the future developments of the study could involve the consideration of a fleet of EV trucks, available at the facility at different time slots, in order to assess the impact of V2G on a larger scale. This analysis will be coupled with the integration within the optimization problem of a MILP formulation of electric trucks' battery degradation cost function, to be included in the objective function. Indeed, the proposed MILP EMS model is general and it could be easily extended to larger facilities, considering different technologies and different units' sizes. Moreover, the participation of EVs in flexibility and ancillary services markets could be investigated, given also the presence of a large wind farm and of a large BESS at the EVCH. The participation in flexibility markets will provide further revenues to the company. Again, the model could be extended with dedicated constraints to manage several EVCHs, participating in flexibility markets in a joint way. Finally, reactive power sharing among the inverters will be a further point of discussion in future studies, in order to ensure a reliable reactive power supply and voltage control for the EVCH.

CRediT authorship contribution statement

Alphonse Francis: Visualization, Methodology, Writing – original draft, Software, Conceptualization. **Matteo Fresia:** Writing – review & editing, Software, Conceptualization, Visualization, Methodology. **Edoardo Barabino:** Resources, Data curation. **Stefano Bracco:** Project administration, Funding acquisition, Supervision, Methodology, Conceptualization.

Declaration of competing interest

The authors declare that they have no known competing financial interests or personal relationships that could have appeared to influence the work reported in this paper.

Acknowledgments

This work is supported by Spoke 10 "Logistics and Freight" within the Italian PNRR National Centre for Sustainable Mobility (MOST), CUP I53C2 2000720001.

Data availability

The data that has been used is confidential.

References

[1] European Commission, Fit for 55 package: delivering the EU's 2030 climate target on the way to climate neutrality, 2021. https://ec.europa.eu/commission/presscorner/detail/en/IP_21_3541.
[2] European Environment Agency, Reducing greenhouse gas emissions from heavy-duty vehicles in Europe, 2022. https://www.eea.europa.eu/publications/co2-emissions-of-new-heavy.
[3] Istituto Superiore per la Protezione e la Ricerca Ambientale (ISPRA), Le emissioni dal trasporto stradale, ISPRA Emission Inventory Website, 2024. https://emissioni.sina.isprambiente.it/le-emissioni-dal-trasporto-stradale/.
[4] European Commission and Directorate-General for Research and Innovation, European Green Deal – Research and Innovation Call, Publications Office of the European Union, 2021, https://doi.org/10.2777/33415.
[5] Italian Ministry of Infrastructure and Transport, Decarbonising transport: scientific evidence and policy proposals, 2024. https://www.mit.gov.it/comunicazione/news/decarbonising-transport-scientific-evidence-and-policy-proposals.
[6] M. Jahangir Samet, H. Liimatainen, O.P.R. van Vliet, GHG emission reduction potential of road freight transport by using battery electric trucks in Finland and Switzerland, Appl. Energy 347 (2023) 121361, https://doi.org/10.1016/j.apenergy.2023.121361.
[7] The Driven, Electric trucks and buses show staggering sales growth in Europe, 2024. https://thedriven.io/2024/03/20/electric-trucks-and-buses-show-staggering-sales-growth-in-europe/.
[8] E. Kallionpää, S. Nair, H. Liimatainen, Perspectives of using electric- and alternatively fuelled freight transport vehicles among road haulage companies in Finland, Transp. Res. Procedia 72 (2023) 1894–1901, tRA Lisbon 2022 Conference Proceedings Transport Research Arena (TRA Lisbon 2022), 14th-17th November 2022, Lisboa, Portugal. https://doi.org/10.1016/j.trpro.2023.11.668.
[9] A. Francis, M. Fresia, S. Bracco, E. Barabino, Optimal operation of an innovative electric vehicle charging hub directly fed by renewables, IFAC-PapersOnLine 58 (2) (2024) 168–173, 3rd IFAC Workshop on Integrated Assessment Modeling for Environmental Systems IAMES 2024, https://doi.org/10.1016/j.ifacol.2024.07.109.
[10] S. Bracco, F. Delfino, F. Pampararo, M. Robba, M. Rossi, Planning and management of sustainable microgrids: the test-bed facilities at the university of genoa, in: 2013 Africon, 2013, pp. 1–5, https://doi.org/10.1109/AFRCON.2013.6757862.
[11] Y. Lavi, J. Apt, Using pv inverters for voltage support at night can lower grid costs, Energy Rep. 8 (2022) 6347–6354, https://doi.org/10.1016/j.egyr.2022.05.004.
[12] M. Shahin, E. Topriska, M. Gormley, M. Nour, Design and field implementation of smart grid-integrated control of pv inverters for autonomous voltage regulation and var ancillary services, Electr. Power Syst. Res. 208 (2022) 107862, https://doi.org/10.1016/j.epsr.2022.107862.
[13] N. Etherden, M.H.J. Bollen, Overload and overvoltage in low-voltage and medium-voltage networks due to renewable energy – some illustrative case studies, Electr. Power Syst. Res. 114 (2014) 39–48, https://doi.org/10.1016/j.epsr.2014.03.028.
[14] International Energy Agency (IEA), Renewables 2022, 2022. https://www.iea.org/reports/renewables-2022.
[15] J. Tant, F. Geth, D. Six, P. Tant, J. Driesen, Multiobjective battery storage to improve pv integration in residential distribution grids, IEEE Trans. Sustain. Energy 4 (1) (2013) 182–191, https://doi.org/10.1109/TSTE.2012.2211387.
[16] A.Y. Ali, A. Hussain, J.-W. Baek, H.-M. Kim, Optimal operation of static energy storage in fast-charging stations considering the trade-off between resilience and peak shaving, J. Energy Storage 53 (2022) 105197, https://doi.org/10.1016/j.est.2022.105197.
[17] A. Zecchino, Z. Yuan, F. Sossan, R. Cherkaoui, M. Paolone, Optimal provision of concurrent primary frequency and local voltage control from a bess considering variable capability curves: modelling and experimental assessment, Electr. Power Syst. Res. 190 (2021) 106643, https://doi.org/10.1016/j.epsr.2020.106643.
[18] S.K. Gupta, T. Ghose, K. Chatterjee, Coordinated control of incentive-based demand response program and bess for frequency regulation in low inertia isolated grid, Electr. Power Syst. Res. 209 (2022) 108037, https://doi.org/10.1016/j.epsr.2022.108037.

[19] M. Fresia, L. Bordo, F. Delfino, S. Bracco, Optimal day-ahead active and reactive power management for microgrids with high penetration of renewables, Energy Convers. Manag. 23 (2024) 100598, https://doi.org/10.1016/j.ecmx.2024.100598.

[20] I. Baghdadi, O. Briat, J.-Y. Delétage, P. Gyan, J.-M. Vinassa, Lithium battery aging model based on dakin's degradation approach, J. Power Sources 325 (2016) 273–285, https://doi.org/10.1016/j.jpowsour.2016.06.036.

[21] C. Bordin, H.O. Anuta, A. Crossland, I.L. Gutierrez, C.J. Dent, D. Vigo, A linear programming approach for battery degradation analysis and optimization in offgrid power systems with solar energy integration, Renew. Energy 101 (2017) 417–430, https://doi.org/10.1016/j.renene.2016.08.066.

[22] M. Petit, E. Prada, V. Sauvant-Moynot, Development of an empirical aging model for li-ion batteries and application to assess the impact of vehicle-to-grid strategies on battery lifetime, Appl. Energy 172 (2016) 398–407, https://doi.org/10.1016/j.apenergy.2016.03.119.

[23] D. Wang, J. Coignard, T. Zeng, C. Zhang, S. Saxena, Quantifying electric vehicle battery degradation from driving vs. vehicle-to-grid services, J. Power Sources 332 (2016) 193–203, https://doi.org/10.1016/j.jpowsour.2016.09.116.

[24] European Commission, Reducing CO_2 emissions from heavy-duty vehicles, 2024. https://climate.ec.europa.eu/eu-action/transport/road-transport-reducing-co2-emissions-vehicles/reducing-co2-emissions-heavy-duty-vehicles_en.

[25] S.E. Ahmadi, M. Marzband, A. Ikpehai, A. Abusorrah, Optimal stochastic scheduling of plug-in electric vehicles as mobile energy storage systems for resilience enhancement of multi-agent multi-energy networked microgrids, J. Energy Storage 55 (2022) 105566, https://doi.org/10.1016/j.est.2022.105566.

[26] S. Limmer, T. Rodemann, Peak load reduction through dynamic pricing for electric vehicle charging, Int. J. Electr. Power Energy Syst. 113 (2019) 117–128, https://doi.org/10.1016/j.ijepes.2019.05.031.

[27] B. Al-Hanahi, I. Ahmad, D. Habibi, M.A.S. Masoum, Smart charging strategies for heavy electric vehicles, eTransportation 13 (2022) 100182, https://doi.org/10.1016/j.etran.2022.100182.

[28] Y. Zhao, M. Noori, O. Tatari, Vehicle to grid regulation services of electric delivery trucks: economic and environmental benefit analysis, Appl. Energy 170 (2016) 161–175, https://doi.org/10.1016/j.apenergy.2016.02.097.

[29] X. Li, Y. Tan, X. Liu, Q. Liao, B. Sun, G. Cao, C. Li, X. Yang, Z. Wang, A cost-benefit analysis of v2g electric vehicles supporting peak shaving in Shanghai, Electr. Power Syst. Res. 179 (2020) 106058, https://doi.org/10.1016/j.epsr.2019.106058.

[30] L.P. Karmali, A. Gholami, N. Nezamoddini, Integrated optimization of production planning and electric trucks charging and discharging scheduling, Sustain. Energy Grids Netw. 39 (2024) 101397, https://doi.org/10.1016/j.segan.2024.101397.

[31] G. Bianco, B. Bonvini, S. Bracco, F. Delfino, P. Laiolo, G. Piazza, Key performance indicators for an energy community based on sustainable technologies, Sustainability 13 (16) (2021) https://doi.org/10.3390/su13168789.

[32] J. Yang, F. Yu, K. Ma, B. Yang, Z. Yue, Optimal scheduling of electric-hydrogen integrated charging station for new energy vehicles, Renew. Energy 224 (2024) 120224, https://doi.org/10.1016/j.renene.2024.120224.

[33] S.S. Deshmukh, J.M. Pearce, Electric vehicle charging potential from retail parking lot solar photovoltaic awnings, Renew. Energy 169 (2021) 608–617, https://doi.org/10.1016/j.renene.2021.01.068.

[34] L. Yao, Z. Damiran, W.H. Lim, Optimal charging and discharging scheduling for electric vehicles in a parking station with photovoltaic system and energy storage system, Energies 10 (4) (2017) https://doi.org/10.3390/en10040550.

[35] T.H.B. Huy, H. Truong Dinh, D. Ngoc Vo, D. Kim, Real-time energy scheduling for home energy management systems with an energy storage system and electric vehicle based on a supervised-learning-based strategy, Energy Convers. Manag. 292 (2023) 117340, https://doi.org/10.1016/j.enconman.2023.117340.

[36] D. Zhang, S. Evangelisti, P. Lettieri, L.G. Papageorgiou, Economic and environmental scheduling of smart homes with microgrid: Der operation and electrical tasks, Energy Convers. Manag. 110 (2016) 113–124, https://doi.org/10.1016/j.enconman.2015.11.056.

[37] Z. Šimić, D. Topić, M. Dubravac, Optimal scheduling of battery energy storage in microgrid to minimize electricity and fuel costs, in: 2022 7th International Conference on Smart and Sustainable Technologies (SpliTech), 2022, pp. 1–6, https://doi.org/10.23919/SpliTech55088.2022.9854260.

[38] S.K. Rai, H.D. Mathur, R.C. Bansal, Optimal energy management of nanogrid using battery storage system, Sustain. Energy Technol. Assess. 55 (2023) 102921, https://doi.org/10.1016/j.seta.2022.102921.

[39] A. Çiçek, Multi-objective operation strategy for a community with ress, fuel cell evs and hydrogen energy system considering demand response, Sustain. Energy Technol. Assess. 55 (2023) 102957, https://doi.org/10.1016/j.seta.2022.102957.

[40] P. Makeen, H.A. Ghali, S. Memon, F. Duan, Smart techno-economic operation of electric vehicle charging station in Egypt, Energy 264 (2023) 126151, https://doi.org/10.1016/j.energy.2022.126151.

[41] A. Dukpa, B. Butrylo, Milp-based profit maximization of electric vehicle charging station based on solar and ev arrival forecasts, Energies 15 (15) (2022) https://doi.org/10.3390/en15155760.

[42] M. Fresia, S. Bracco, Electric vehicle fleet management for a prosumer building with renewable generation, Energies 16 (20) (2023) https://doi.org/10.3390/en16207213.

[43] S. Bracco, M. Fresia, Energy management system for the optimal operation of a grid-connected building with renewables and an electric delivery vehicle, in: IEEE EUROCON 2023 - 20th International Conference on Smart Technologies, 2023, pp. 472–477, https://doi.org/10.1109/EUROCON56442.2023.10198884.

[44] I. Keskin, G. Soykan, Optimal cost management of the cchp based data center with district heating and district cooling integration in the presence of different energy tariffs, Energy Convers. Manag. 254 (2022) 115211, https://doi.org/10.1016/j.enconman.2022.115211.

[45] A. Çiçek, Optimal operation of an all-in-one ev station with photovoltaic system including charging, battery swapping and hydrogen refueling, Int. J. Hydrogen Energy 47 (76) (2022) 32405–32424, https://doi.org/10.1016/j.ijhydene.2022.07.171.

[46] E. Srilakshmi, S.P. Singh, Energy regulation of ev using milp for optimal operation of incentive based prosumer microgrid with uncertainty modelling, Int. J. Electr. Power Energy Syst. 134 (2022) 107353, https://doi.org/10.1016/j.ijepes.2021.107353.

[47] M. Fresia, T. Robbiano, M. Caliano, F. Delfino, S. Bracco, Optimal operation of an industrial microgrid within a renewable energy community: a case study of a greentech company, Energies 17 (14) (2024) https://doi.org/10.3390/en17143567.

[48] N. Blasuttigh, S. Pastore, M. Scorrano, R. Danielis, A.M. Pavan, Vehicle-to-ski: a v2g optimization-based cost and environmental analysis for a ski resort, Sustain. Energy Technol. Assess. 55 (2023) 102916, https://doi.org/10.1016/j.seta.2022.102916.

[49] A. Francis, M. Fresia, S. Bracco, E. Barabino, Energy management system for the operation of an electric vehicle charging hub fed by solar and wind energy sources, in: 2024 IEEE International Conference on Environment and Electrical Engineering and 2024 IEEE Industrial and Commercial Power Systems Europe (EEEIC / ICPS Europe), 2024, pp. 1–7, https://doi.org/10.1109/EEEIC/ICPSEurope61470.2024.10751396.

[50] Comitato Elettrotecnico Italiano (CEI), CEI 0-16: technical rules for the connection of active and passive users to the HV and MV electrical networks of distribution companies, standard document (2022, https://mycatalogo.ceinorme.it/cei/item/0000018527.

[51] Autorità di Regolazione per Energia Reti e Ambiente (ARERA), Delibera 712/2022/R/eel: Dettaglio Atti e Provvedimenti, 2022. https://www.arera.it/atti-e-provvedimenti/dettaglio/22/712-22.

[52] M. Mattei, G. Notton, C. Cristofari, M. Muselli, P. Poggi, Calculation of the polycrystalline pv module temperature using a simple method of energy balance, Renew. Energy 31 (4) (2006) 553–567, https://doi.org/10.1016/j.renene.2005.03.010.

[53] J.A. Duffie, W.A. Beckman, N.E. Blair, Design of Photovoltaic Systems, John Wiley & Sons, Ltd, 2020, Ch. 23, pp. 760–788. https://doi.org/10.1002/9781119540328.ch23.

[54] T. Huld, R. Müller, A. Gambardella, A new solar radiation database for estimating pv performance in Europe and Africa, Sol. Energy 86 (6) (2012) 1803–1815, https://doi.org/10.1016/j.solener.2012.03.006.

[55] L. Pagnini, S. Bracco, F. Delfino, M. de Simón-Martín, Levelized cost of electricity in renewable energy communities: uncertainty propagation analysis, Appl. Energy 366 (2024) 123278, https://doi.org/10.1016/j.apenergy.2024.123278.

[56] A. Leippi, M. Fleschutz, K. Davis, A.-L. Klingler, M.D. Murphy, Optimizing electric vehicle fleet integration in industrial demand response: maximizing vehicle-to-grid benefits while compensating vehicle owners for battery degradation, Appl. Energy 374 (2024) 123995, https://doi.org/10.1016/j.apenergy.2024.123995.

[57] J. Löfberg, Yalmip: a toolbox for modeling and optimization in matlab, in: Proceedings of the CACSD Conference, Taipei, Taiwan, 2004.

[58] Gurobi Optimization, LLC, Gurobi Optimizer Reference Manual, 2024. https://www.gurobi.com.

[59] HOMER Energy by UL, HOMER Grid, Version 2.11, HOMER Energy, Boulder, CO, USA, 2023. https://www.homerenergy.com.